Multispectral Software Development for the Airborne Bathymetric Survey System

M. T. Kalcic
S. C. Lingsch
Mapping, Charting, and Geodesy Division
Ocean Science Directorate

Foreword

Hydrographic and bathymetric charts of the world's coastal waters are essential to the missions of many U.S. Navy programs. A coastal survey requirements study by the Defense Mapping Agency (DMA) showed a 200- to 300-year backlog if the necessary bathymetry data are to be gathered by conventional ship surveying methods.

The Mapping, Charting, and Geodesy (MC&G) Division of the Naval Oceanographic and Atmospheric Research Laboratory (NOARL) was tasked to develop the Airborne Bathymetric Survey (ABS) system and its supporting software. In response, the MC&G Division produced the ABS system design, the NOARL Scanner, and a laser sounder. These instruments, together with a global positioning system and an inertial navigation system aboard a U.S. Navy P-3 aircraft, are intended to survey clear, shallow coastal waters. In addition, software was written to process the multispectral data provided by the NOARL Scanner and to calculate the shallow-water bathymetry based on laser- and boat-derived soundings.

The instrumentation, the software, and the algorithms that resulted from this effort are described in this report. This advanced technology could reduce the DMA survey data backlog and help provide current, high-resolution hydrographic and bathymetric data to users.

W. B. Moseley
Technical Director

L. R. Elliott, Commander, USN
Commanding Officer

DISCLAIMER NOTICE

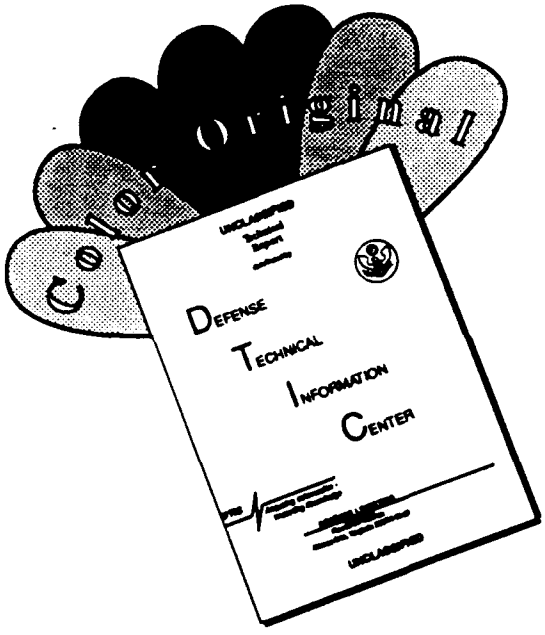

THIS DOCUMENT IS BEST QUALITY AVAILABLE. THE COPY FURNISHED TO DTIC CONTAINED A SIGNIFICANT NUMBER OF COLOR PAGES WHICH DO NOT REPRODUCE LEGIBLY ON BLACK AND WHITE MICROFICHE.

Executive Summary

The Mapping, Charting, and Geodesy (MC&G) Division of the Naval Oceanographic and Atmospheric Research Laboratory's Ocean Science Directorate is the primary activity within the U.S. Navy for conducting research and development in direct support of naval MC&G requirements. The Mapping Sciences Branch of the MC&G Division was tasked to develop the algorithms and software necessary to process data and to produce bathymetry from the multispectral scanner of the Airborne Bathymetric Survey system when it becomes fully functional. The software developed for this system is called the Multispectral Image Depth Analysis System, or MIDAS. The software processes multispectral data in conjunction with laser- or boat-derived soundings to produce high-resolution bathymetric grids. The system is designed to estimate depths in clear, shallow coastal waters down to 20 m. The depth accuracies, derived from the system using boat soundings for control, ranged from 0.3 m to 1.4 m in waters extending to 3 m and 10 m, respectively. The horizontal positioning accuracy of the system was in the 25-m range, as determined from a ground survey.

Acknowledgments

This project was initially funded by the Defense Mapping Agency under Program Element 63701B, with final funding from the Chief of Naval Operations (CNO OP-096) under program element 63704N. We thank these sponsors for their support.

In addition, many people contributed to the project: Dr. Stephen Haimbach, former principal investigator (now with Pacific Sierra Research); Mr. Michael Harris, Head, MC&G Division, NOARL, who preceded Dr. Haimbach as the principal investigator; and Dr. Charles Walker who contributed to bathymetric algorithm development. We also thank Mr. Jerry Bymes, NOARL; Dr. Temple Fay, University of Southern Mississippi; Mr. Vincent Miller, NOARL; Dr. Kent Clark, University of South Alabama; Dr. Andrew Martinez, Tulane University; and Mr. Richard Joy, now with the Army Environmental Topographic Laboratory. We also acknowledge the support of Dr. Daniel Hickman, former Head, MC&G Division, and of Dr. Herbert C. Eppert, Jr., Director, Ocean Science Directorate.

Special thanks go to Mr. Hillary Mesick of NOARL, for his practical wisdom and professional advice on the software and algorithms. The authors also express thanks to Mr. Lockwood Peckinpaugh and Mr. John Casey of Sverdrup Technology for software development, and to Mr. Julius Bayham of Lockheed for tape decommutation and processing.

The mention of commercial products or the use of company names does not in any way imply endorsement by the U.S. Navy or NOARL.

Contents

Introduction 1

Operational Requirements 1

Processing Requirements 1

The NOARL Scanner 2

Multispectral Image Depth Analysis System 3
Preprocessing 3
MIDAS Processing System 3

Results 8
Data Registration and Rectification Results 8
Glint Correction Results 9
Depth Estimate Results 15
CPU Time 15

Summary 15

Recommendations 17

References 19

Appendix A. NOARL Scanner System and Specifications 21

Appendix B. Algorithms and Techniques 25

Appendix C. Depth File Format 41

Multispectral Software Development for the Airborne Bathymetric Survey System

Introduction

This report presents the results of the scanner software and algorithm development for the Airborne Bathymetric Survey (ABS) System developed by the Naval Oceanographic and Atmospheric Research Laboratory (NOARL).* A brief background of the development of the system and its scope and objectives is given, followed by the results of the scanner software effort.

The ABS system comprises a hydrographic airborne laser sounder (HALS), a multispectral scanner (MSS), a global positioning system (GPS), and an inertial navigation system (INS) on board a Navy P-3 hydrographic airplane. The Naval Air Development Center (NADC) installed the hardware aboard the P-3. Figure 1 depicts the positioning of the system components on board the aircraft. The NOARL Scanner (NS) is located on the center line of the plane aft of the laser sounder system. The system is designed to collect hydrographic information over clear, coastal waters at depths up to 20 m.

The ABS system resulted from three developments: a requirement for hydrographic and bathymetric information from the world's coastal areas that is essential to the mission of many Navy programs; a Defense Mapping Agency (1978) coastal survey requirements study that showed a conventional survey-ship backlog of 200 to 300 years, or 8250 nmi^2; and advances in laser and satellite technology that made the ABS system an achievable goal (Polcyn, 1976; Enabnit, 1979; Compton, 1988).

The system was developed in two phases. Phase I MSS development was to assemble and test a nine-channel scanner and data processing algorithms to meet operational requirements (discussed later). A description of Phase I for the multispectral software is given by Kalcic et al. (1989). Phase II development was to enhance algorithms and computer software necessary to fully position and process scanner data to approach International Hydrographic Office (IHO) standards.

*Formerly the Naval Ocean Research and Development Activity (NORDA).

Operational Requirements

ABS system accuracy requirements must meet IHO standards (Table 1) and ensure the detection of all hazards. To provide a high likelihood of hazard detection, the pixel size of the MSS was required to be 1 m or less, so that such a feature would be spread over at least five pixels. The ABS system was also required to provide 200% coverage of the bottom because of the possibility that noise would mask subsurface hazards. The Naval Oceanographic Office (NAVOCEANO) plans to obtain that coverage by flying the system in two successive flight lines spaced 250 m apart. The line spacing and the overlap require a swath width of at least 500 m. This width is achieved by having a field of view of 54 degrees or larger. In addition to the parallel flight lines, cross-check lines will be flown approximately 2500 m apart.

Processing Requirements

The ABS system is expected to operate an average of 160 to 200 hours per year. The processing requirements for the NS data stem from the collection rate of 100 scanlines per second. Data collected average 36,000 scanlines per hour, or 7,200,000 scanlines per year or 331.776 Gbytes per year. To process all the data, the daily processing requires that 28,800 scanlines, over fifty 512×512 byte images, each with five channels, be processed each day (based on 250 working days/year).

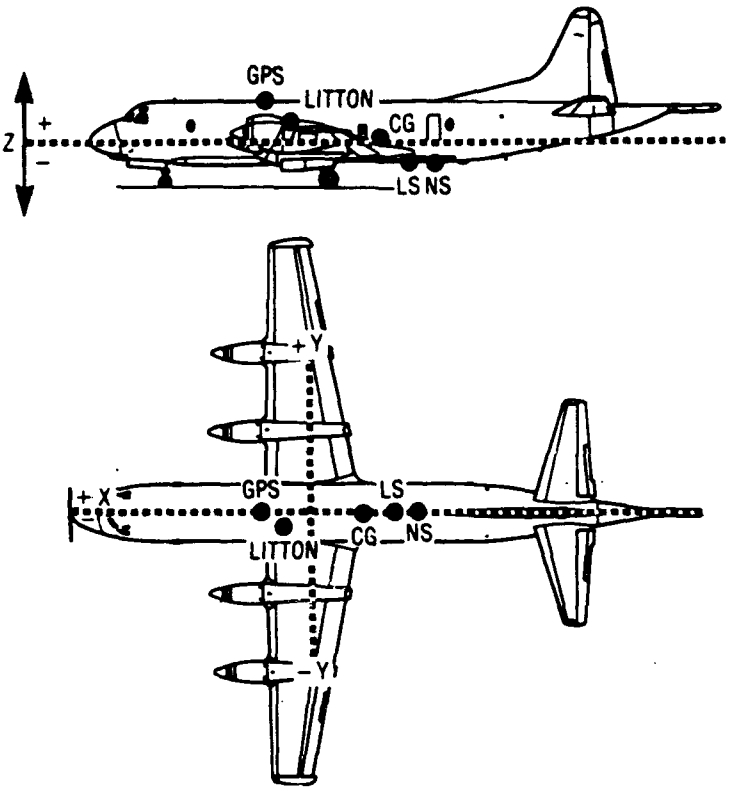

	X	Y	Z
Reference	Nose of Aircraft	Aircrafts Center Line	Deck
GPS receiver	+265"	0	+84"
Litton 72	+320"	−38.5"	+25"
Laser sounder	+758"	0	−34.5"
NS scanner	+791"	0	−34.5"
Center of gravity	+621"	0	0

Figure 1. ABS system configuration on board a P-3 aircraft. The displacements of the system components from a point in the center of the aircraft are given as x, y, and z in the table. The system also has recorders on board.

The NOARL Scanner

The NS is a 9-channel MSS with increased sensitivity in the blue-green portion of the spectrum. Schematic representations and specifications for the NS are given in Appendix A.

The spectral resolution of the NS is given in Table 2. Bands 1–6 are visible light bands and bands 7–9 are infrared bands. The NS spectral bandwidths are similar to National Aeronautics and Space Administration's (NASA) Landsat Thematic Mapper (TM), except that the first four bands of the NS, the water-penetrating bands, make up the first two bands of the TM. NS bands 5–9 are equivalent to TM bands 4–7.

The data are recorded on a 14-track, high-density tape on board the aircraft. The high-density tapes are decommutated to 6250-bpi density computer compatible tapes (CCT). Table 3 shows the format of the data records on the 6250-bpi tapes.

Table 1. ABS system operational requirements.

Requirement	Threshold	
	(Based on IHO Standards)	(Based on NAVOCEANO Requirements)
Positioning	15-m platform relative to shore 5-m sensor relative to platform	
Depth Determination	± 0.3 m in depths 0 – 30 m ± 1.0 m in depths 30 – 100 m ± 1% in depths greater than 100 m	
Hazard Detection		Minimum Target Size is 5-m diameter in depths less than 20 m
Least Depth Determination		100% spatial coverage

Table 2. Spectral bandwidths of the NOARL scanner.

Band	Spectral Band
1	450 – 480 nm*
2	450 – 520 nm
3	520 – 550 nm
4	550 – 600 nm
5	630 – 690 nm
6	760 – 900 nm
7	1.55 – 1.75 μm**
8	2.08 – 2.35 μm
9	10.4 – 12.5 μm

*nm nanometers
**μm micrometers

Multispectral Image Depth Analysis System

The Multispectral Image Depth Analysis System (MIDAS) is a software system that processes the multispectral data to produce high-resolution bathymetric grids. The system consists of 11,000 lines of Fortran 77 source code, making up 109 programs and subroutines. Appendix B describes the algorithms and techniques that are used in MIDAS software. Kalcic et al. (1988) list the source codes and provide user documentation for the software. These methods result from much of the work done in Phase I of the ABS system development (Kalcic et al., 1989) and continued in Phase II.

The Phase II software implementation of the algorithms is described in this section. The software is divided into two major processing areas. The first process, the deblocking procedure, divides continuous flight lines into subareas and preprocesses the navigation. The second process rectifies the multispectral image for attitude distortion; registers it to a 1-m, equal-area projection grid; maps laser-derive derived depths to the multispectral image; and calculates depths and outputs them to an image file. Figure 2 is an operational diagram for MIDAS.

Preprocessing

The deblocking procedure, DEBLOCK, reads the decommutated tape, and divides one flight line into manageable subareas. This procedure operates in batch mode. The size of the subareas is adjustable, but 512 × 624 pixels or 0.5 × 0.6 km, was convenient because most image display devices are capable of 512 × 512 pixel display. Navigation and attitude data are validated and a position is computed for each scanline by module GEONAV. At completion, a file of subareas is generated for input to the MIDAS processing system.

MIDAS Processing System

MIDAS performs the geometric corrections (GEORECT), maps the laser-derived depths to the multispectral image (GEOMATCH), performs the depth calculations (least-mean-square (LMS) or DEEP), and outputs a depth file. MIDAS allows the analyst to view the data before processing and to view the results after each process. MIDAS has the option to run in two modes: interactive or production. A flow diagram in shown in Figure 3.

Modes of Operation

Interactive mode. This option allows the analyst to view the MSS data prior to processing, or the results at any step. The analyst has the option of processing any subarea within the flight line and

Table 3. NS data format (1 record of 6250 bpi tape).

Word	Byte	Parameter	Bits	Description
1	0	Spare	0–7	
	1	Scan Line Count	0–3	10,000's
	1	"	4–7	100,000's
	2	"	0–3	100's
	2	"	4–7	1,000's
	3	"	0–3	1's
	3	"	4–7	10's
2	0	Spare	0–7	
	1	Scan Speed	0	100's of scans/sec
	1	"	1–7	unused
	2	"	0–3	1's of scans/sec
	2	"	4–7	10's of scans/sec
	3	Spare	0–7	
3	0	Roll	0–5	6 MSB's[1] of 14
	0	"	6–7	bit 6 is unused validity bits
	1	"	0–7	8 LSB's[2] of 14
	2	Pitch	0–5	6 MSB's of 14
	2	"	6–7	bit 6 is unused validity bits
	3	"	0–7	8 LSB's of 14
4	0	Shot Time	0–1	2 MSB's of 10 of msec
	0	"	2–5	4 bits of sec
	0	"	6–7	bit 6 is unused validity bits
	1	"	0–7	8 LSB's of 20 of msec
	2	Spare	0–7	
	3	Time	0–1	2 MSB's of 10 of msec
	3	"	2–6	unused
	3	"	7	MSB of 17 of sec
5	0	"	0–7	8 LSB's of 10 of msec
	1	"	0–7	bits 8–15 of 17 of sec
	2	"	0–7	8 LSB's of 17 of sec
	3	Altitude	0–7	8 MSB's of 16
6	0	"	0–7	8 LSB'sF of 16
	1	Drift Angle	0–7	8 MSB's of 16
	2	"	0–7	8 LSB's of 16
	3	True Heading	0–7	8 MSB's of 16
7	0	"	0–7	8 LSB's of 16
	1	Latitude	0–7	8 bit exponent of 48 bit FP[3]
	2	Latitude	0–7	bits 32–39 of 40 bit mantissa
	3	"	0–7	bits 40–47 of 40 bit mantissa
8	0	"	0–7	bits 16–23 of 40 bit mantissa
	1	"	0–7	bits 24–31 of 40 bit mantissa
	2	"	0–7	bits 0–6 of 40 bit mantissa
	3	Longitude	0–7	8 bit exponent of 48 bit FP
9	0	"	0–7	bits 32039 of 40 bit mantissa
	1	"	0–7	bits 40–47 of 40 bit mantissa
	2	"	0–7	bits 16–23 of 40 bit mantissa
	3	"	0–7	bits 24–31 of 40 bit mantissa
10	0	"	0–7	bits 0–6 of 40 bit mantissa
	1	Horizontal Velocity	0–7	8 bit exponent of 32 bit FP
	2	"	0–7	bits 16–23 of 40 bit mantissa
	3	"	0–7	bits 24–31 of 40 bit mantissa
11	0	"	0–7	bits 0–6 of 24 bit mantissa
	1	Direction	0–7	8 bit exponent of 32 bit FP
	2	"	0–7	bits 16–23 of 24 bit mantissa
	3	"	0–7	bits 24–31 of 24 bit mantissa

[1] most significant bit [2] least significant bit [3] floating point

Table 3. Continued.

Word	Byte	Parameter	Bits	Description
12	0	"	0–7	bits 0–6 of 24 bit mantissa
	1	GPS Time at Solution	0–7	8 bit exponent of 48 bit FP
	2	"	0–7	bits 32–39 of 40 bit mantissa
	3	"	0–7	bits 40–47 of 40 bit mantissa
13	0	"	0–7	bits 16–23 of 40 bit mantissa
	1	"	0–7	bits 24–31 of 40 bit mantissa
	2	"	0–7	bits 0–6 of 40 bit mantissa
	3	BB1 Temp	0–2	10's of degrees
	3	"	3	sign (0=+)
	3	"	4–7	unused
14	0	"	0–3	0.1's of degrees
	0	"	4–7	1's of degrees
	1	BB2 Temp	0–2	10's of degrees
	1	"	3	sign (0=+)
	1	"	4–7	unused
	2	"	0–3	0.1's of degrees
	2	"	4–7	1's of degrees
	3	Image Data (700 bytes)		1 byte pixels
15	0			
189	3	BB1 Radiant Temperature	0–7	
190	0	Sphere	0–7	
	1	BB2 Radiant Temperature	0–7	
	2	Gain	0–3	
	2	Channel ID	4–7	
	3	Fill Pattern	0–7	55 (hex)

of setting processing limits within the subarea. Setting processing limits within the subarea allows the analyst to eliminate image portions that are contaminated with sun glint/glare or are of poor quality for other reasons.

Production mode. This option allows the analyst to set initial parameters—i.e., region of interest, starting subarea. Successive subareas are processed until the end of the flight line is reached.

Data Storage

MIDAS contains three common data areas: static, dynamic, and scratch. The static area contains data structures that remain constant throughout processing. The dynamic area contains data structures that may change between modules. The scratch area is for mapping local variables into memory. This area of memory is used repeatedly by various routines, so it is referred to as "scratch" memory. All data, including image data for the subarea being processed, reside in memory at all times. This data storage capability requires a large program size (e.g., 12 Mbytes for 6 multispectral channels). The tradeoffs are that data input and output (I/O) are reduced and the storage of intermediate files need not be eliminated. The display portion of MIDAS reads the data directly from memory, which also reduces I/O.

Modules Description

PNAV. Module PNAV is part of the deblocking process. PNAV reads the magnetic tape file and loads the image and navigation data into a common memory area.

Each time PNAV is invoked, a subarea is loaded into the common area. For the first subarea, scanlines are searched until the millisecond portion of the shot-time is zero. This event is defined as a shot-time rollover. This scanline contains the first navigation position so this is where processing starts.

As each scanline is read the image data are read into common memory in 2-byte or 16-bit variables. The extra space is allotted to handle the Airborne Multispectral Pushbroom Scanner (AMPS) 12-bit data. The navigation data unpacking is done at this point. Only those fields used in processing are unpacked. They include latitude, longitude, GPS heading, INS heading, GPS time, shot time, roll,

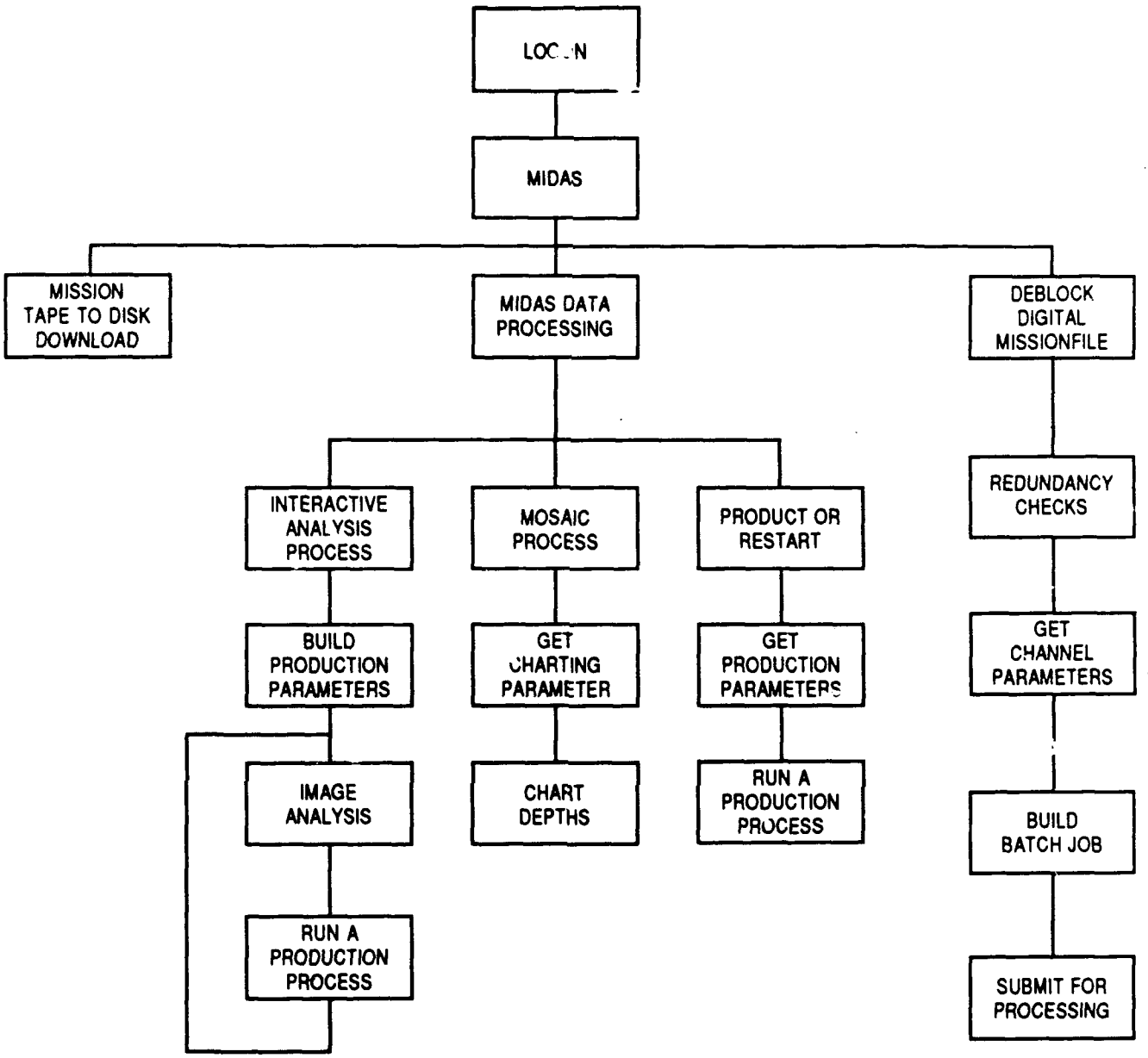

Figure 2. Operational diagram for MIDAS.

pitch, and drift. The image and navigation data are read until enough lines for a subarea plus an overlap area or the end of the flight line is encountered. The navigation data are read until shot-time rollover is found. The overlap data are stored in local buffers, which are read in when the successive area is processed.

GEONAV. Module GEONAV is part of the deblocking process. Aircraft navigation and attitude data are checked for validity. The GPS parameters of latitude, longitude, and heading are shifted back 2 seconds to account for the time delay in receiving them. A time and a position are computed for each scanline.

A data validity mask is built by scanning the GPS times. A GPS time of zero denotes a data dropout. In the event of a dropout, it is assumed that all parameters received over the slow bus (Kalcic et al., 1989), which includes latitude, longitude, altitude, drift, INS heading, and GPS heading, are invalid. The previous GPS times are scanned until a valid GPS time is encountered. A valid time is computed by linear interpolation as a function of scan rate.

Altitude, drift, and INS heading are replaced by the closest valid value. Latitude, longitude, and GPS heading are valid only when the millisecond portion of the shot time goes to zero. The shot time is a

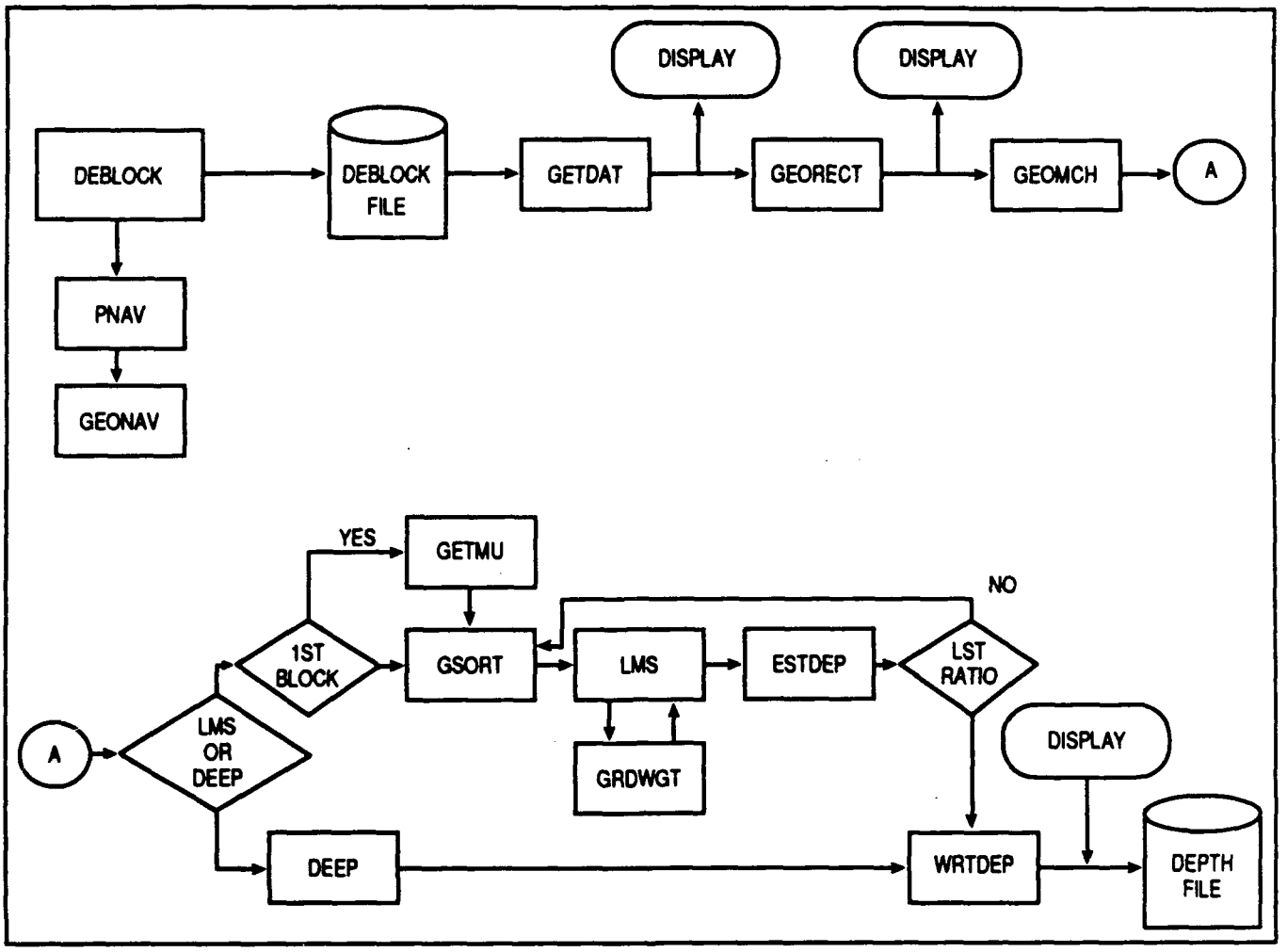

Figure 3. MIDAS flow diagram.

time-keeping parameter used to flag GPS readings. The shot-time clock resets to zero whenever a GPS value becomes valid. The parameters are replaced only when a data dropout occurs during a rollover.

Aircraft attitude is scanned for noise spikes. A difference threshold of 0.5 degree for roll, pitch and drift and a difference threshold of 100 m for altitude are used to flag spikes. When a spike occurs the parameter is replaced by the previous valid value.

The shot time received over the fast bus (Kalcic et al., 1989) is updated every scanline. If an update does not occur, then the time is replaced by linear interpolation.

A time is generated for each scanline using the GPS time and the shot time. The initial time is the GPS time at the first shot-time rollover of the flight line. Successive times are incremented from the initial time.

The GPS parameters, latitude, longitude, and heading, are updated approximately every second. With a scan rate of 100 lines per second, a positional update occurs every 100 scan lines. These parameters become valid at the shot-time rollover. If the first block within the flightline is being processed, then it is assumed that the first line has a shot time of zero. If the first block is not being processed, the first scanline has a valid position computed from the previous block. The data are then scanned for a second shot-time rollover. The data validity flag is checked. If the data are invalid, then the next rollover is found with valid data. Up to 5 seconds of data can be interpolated. When two valid positions are found, a linear interpolation is performed.

Roll, pitch, and drift are updated every 100 msecs or every 10 scanlines. These parameters are low pass filtered using a 13-point Martin filter with a frequency cutoff of 0.05 cycles/0.01 seconds.

GEORECT. Module GEORECT geometrically corrects the multispectral image for aircraft attitude (roll, pitch, and drift). Mapping coefficients are

computed by using the image boundaries and the interior positions as control points (see App. B). Geometric corrections are performed on each pixel. The corrected pixels are mapped to a 1-m grid via the mapping equations. Oversampling and changes in the roll, pitch, and drift angles may cause more than one pixel to occupy the same cell. In these cases the digital count values are averaged. At this point, land is identified and mapped to the grid and invalid data are rejected.

The distance between the center of pixels increases as the distance from nadir increases; i.e., at an altitude of 500 m this distance becomes 1.7 m at the outermost edge. When sampled to a 1-m grid, this effect causes data gaps along the scanline. Data gaps between scan lines may occur, depending on sampling rate, air speed, and changes in aircraft attitude. Nearest-neighbor resampling is used to fill in these data gaps. Only those pixels that have adjacent neighbors are resampled; otherwise, a depth is not computed for that position. The order of the nearest neighbor search is as follows: left, right, below, above, lower left, lower right, upper left, upper right.

Band 6 (760–900 nm) is used as a land mask channel. A threshold is determined prior to processing. When the digital count in channel 6 exceeds the threshold, its location is determined in the grid and all bits are set denoting land. Data points with values of 0 or 255 are flagged as invalid. Their position on the grid is computed and the high bit in the word is set.

At the completion of this module, each pixel can be addressed by latitude and longitude via the mapping equations.

GEOMATCH. Module GEOMATCH registers laser- or sonar-derived control points to the rectified multispectral image. The registration is accomplished by using the mapping coefficients computed in module GEORECT.

The module has the option to either search a portion of the laser sounder file or search the entire file for soundings that lie within the image boundaries. If laser data were collected concurrently with the multispectral data, then only that portion of the file is searched. A time interval is computed based on the aircraft's speed, altitude, and laser angle to insure no laser sounder depths are lost due to the laser sounder leading or trailing the aircraft. Since the laser sounder file is sorted by time, the search time is significantly reduced. To handle the case where laser sounder data may have been collected at different times, the file is searched sequentially.

Other data sources (i.e., data collected from ships) can also be used by this module. The data necessary are latitude, longitude and depth. The module matches the corresponding pixel values based on the mapping equations and outputs a data set for input into the depth modeling programs.

LMS. LMS uses the control data from the GEOMATCH program to compute weights for depth estimation (Martinez, 1988; see App. B). The weights are gridded to produce a weight matrix, which is then multiplied by a pixel matrix to produce depths. In the case of more than one channel, several matrices are computed. The gridding of the weights is a lengthy process and where no overlap is present on the image edges, gridding of the weights is not recommended. There is simply not enough data to accurately grid the weights. This factor is a problem with the LMS algorithm.

DEEP. DEEP uses multiple regression methods (Clark, 1988; see App. B) to compute weights for depth estimation. A Cholesky decomposition is used for rapid solution of a system of simultaneous equations and to produce a least-squares solution for the depth mapping coefficients These coefficients are multiplied with the image to produce depths.

The resulting depths are output in image file format (described in App. C). The depths are multiplied by 10, so that 0.1-m precision is retained in the output. The depths range from 0 to 200, representing depths from 0 to 20 m. The present system outputs depths to a 1-m grid, although user-requested output resolution is allowed.

Results

Data Registration and Rectification Results

Test flights with GPS coverage were based upon a Rockwell Collins GPS 1.023 MHz clear acquisition (C/A) ranging signal code receiver provided by the Naval Air Development Center (NADC) and installed on the BIRDSEYE P-3 aircraft. The positioning available from C/A codes is less accurate than the 10.23-MHz precision (P) ranging signal to be used operationally. This reduction in aircraft positioning accuracy reduces overall registration accuracy computed from test data sets.

The data used to verify the attitude correction algorithms were collected over Slidell, Louisiana (near New Orleans). Sidewalks and driveway intersections, easily located on the multispectral

Table 4. Ground truth evaluation of corrected GPS positions from aircraft readings. Results are given in meters.

Station	X Error	Y Error	Total Error (m)
1	18.4	27.6	33.1
2	25.7	4.2	26.0
3	26.4	11.7	28.9
4	24.2	16.3	29.2
5	13.2	15.3	20.2
6	11.7	16.1	19.9
7	2.2	23.1	23.2
8	13.2	32.4	35.0
9	22.6	14.8	27.0
10	21.3	1.7	21.4
11	13.9	8.9	16.5
12	0.7	7.6	7.6
13	6.6	8.0	10.4
14	2.2	12.0	12.2
15	6.6	15.5	16.8
16	14.7	31.4	34.7
17	7.3	26.3	27.3
18	7.3	34.1	34.9
19	19.1	30.7	36.1

image, were chosen as ground stations. These landmarks were well distributed throughout the image. Geographic positions at the ground stations were collected using a Motorola Mini Ranger Eagle GPS receiver.

The pixel location of the ground station was found on the multispectral image. The corresponding latitude and longitude were computed using the set of mapping coefficients computed for the image. Table 4 shows the results at 19 locations. The X and Y errors are the distances in meters in the east-west and north-south directions, respectively, between the image-computed position and the ground station GPS reading. The total error is the straight line distance in meters. The original and rectified images are shown in Figure 4.

The root-mean-square (rms) error of 25.7 m is based on the deviation of the computed pixel location from the averaged GPS location of that pixel on the ground. Many sources of error are inherent in this value; therefore, this rms is not a true measurement of the model error. The accuracy of GPS positions depends on the position dilution of precision (PDOP). The PDOP is a measure that relates the configuration geometry of the GPS satellites to the positioning accuracy (Wells, 1986). The positioning accuracy is a product of the PDOP and the measurement accuracy. Since the PDOP was not available for the aircraft data and was not recorded in the field experiments, the actual positioning accuracy could not be measured for this experiment. The measurement accuracy for the GPS ground readings was measured, however, by recording several readings while the receiver was stationary and the PDOP was not changing. An observation was that the high variability was due to differing PDOPs on different days recorded at the same location. In most cases, there was more day-to-day variability than variability due to the model estimates.

The registration algorithms were applied to data collected over shallow waters in the Florida Keys. The study area is shown in the dashed box in Figure 5. The laser and multispectral image registration in Figure 6 is for a 500-m^2 area off the Eastern Sambo Shoals. Since the laser positions were not validated with control points, the accuracy of this registration could not be determined.

Glint Correction Results

Two independent data sets were flown on different days off Panama City, Florida, and Key West, Florida. Both data sets were collected using the NS. Different solar elevation angles were used to study glint (Lingsch, 1989). The Panama City data were collected in the spring of 1988, and the Key West data were collected in the summer of 1988. Figures 7 through 10 represent true-color images of bands 2, 4, and 5. Figures 7 and 9 are the raw data. Figures 8 and 10 are the corrected data for glint removal. In each case the deep-water region used for the model was a subsampled 512×512 pixel scene or 3500 data points.

The Panama City corrected data set (Fig. 8) exhibits a visual improvement over the raw data. Several pixels on the far right were not corrected because they did not meet the criteria for a glint-contaminated pixel. The offshore bar was preserved, whereas much of the "white water," or breaking waves, was corrected. Some of the vegetation and roads were processed as water pixels because the signal in the near-infrared images (band 6) over these regions fell above the glint and below the land thresholds.

The Key West corrected data set (Fig. 10) reveals bottom features not easily apparent in Figure 9. These features appear to be of the same intensity as similar features that appear in the nonglinted

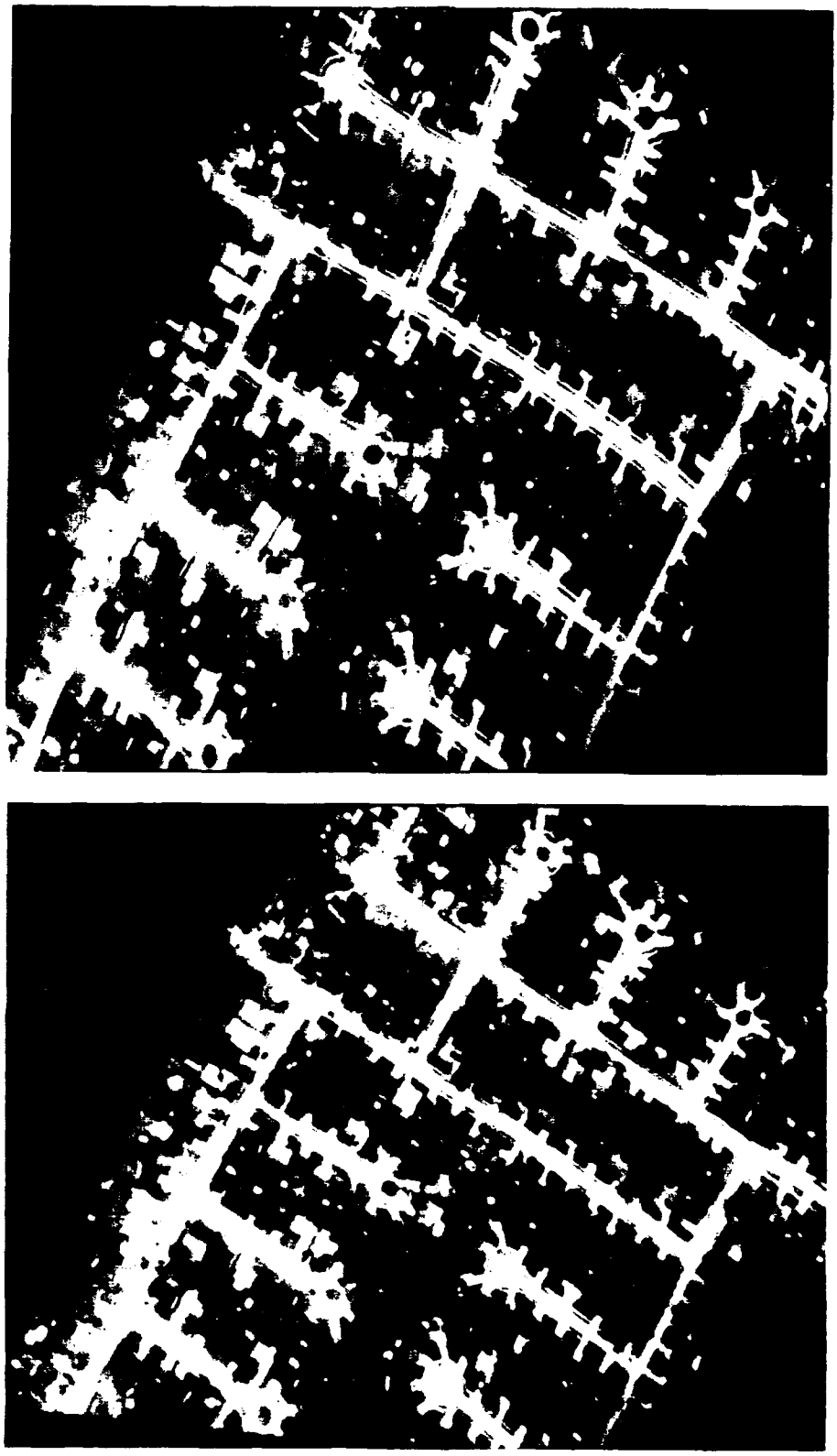

Figure 4. Example of NS image over Slidell, before (top) and after (bottom) geometric rectification.

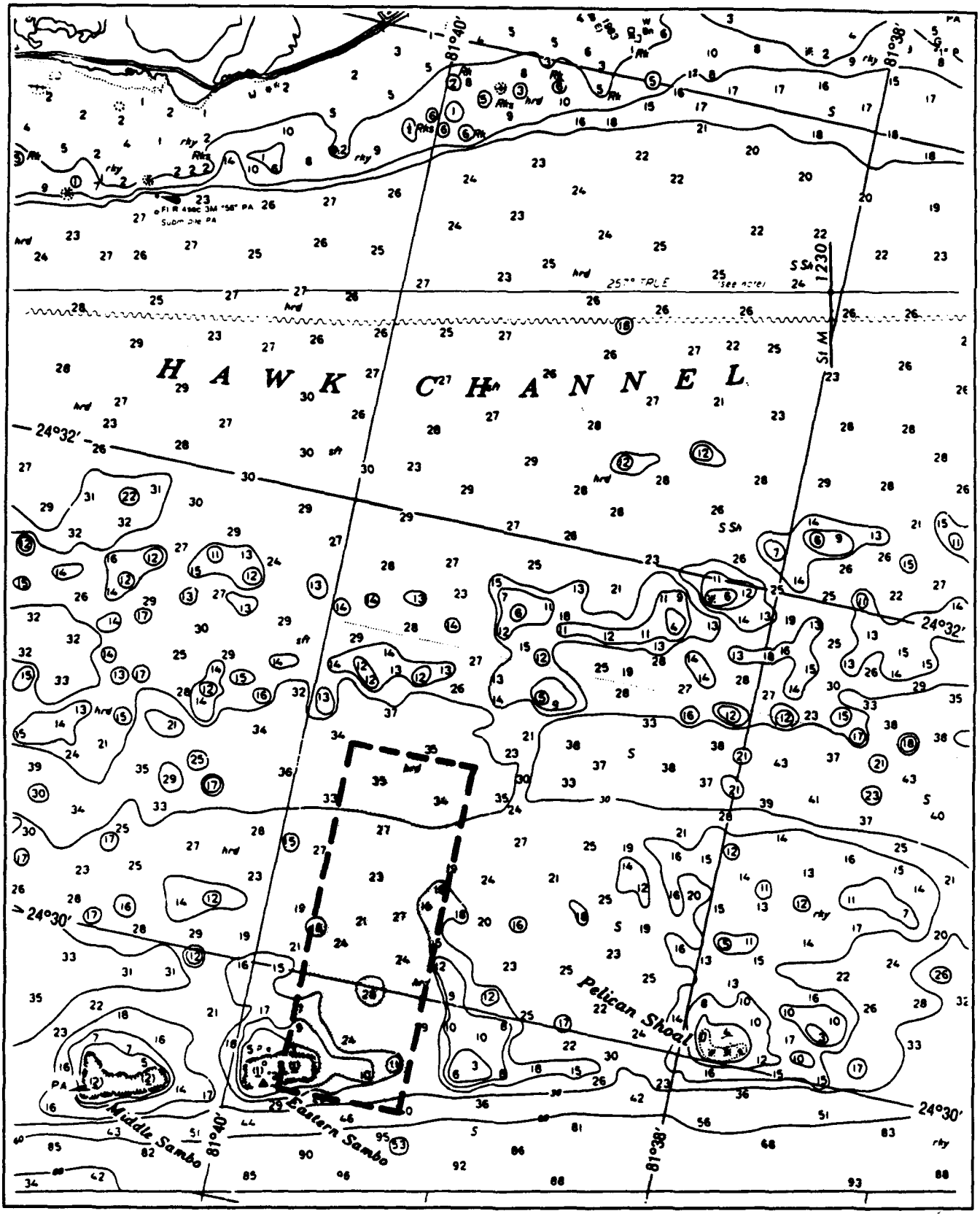

Figure 5. Study area south of Key West, represented by dashed lines on 1:40,000 scale NOAA chart no. 11445. Soundings are shown in feet.

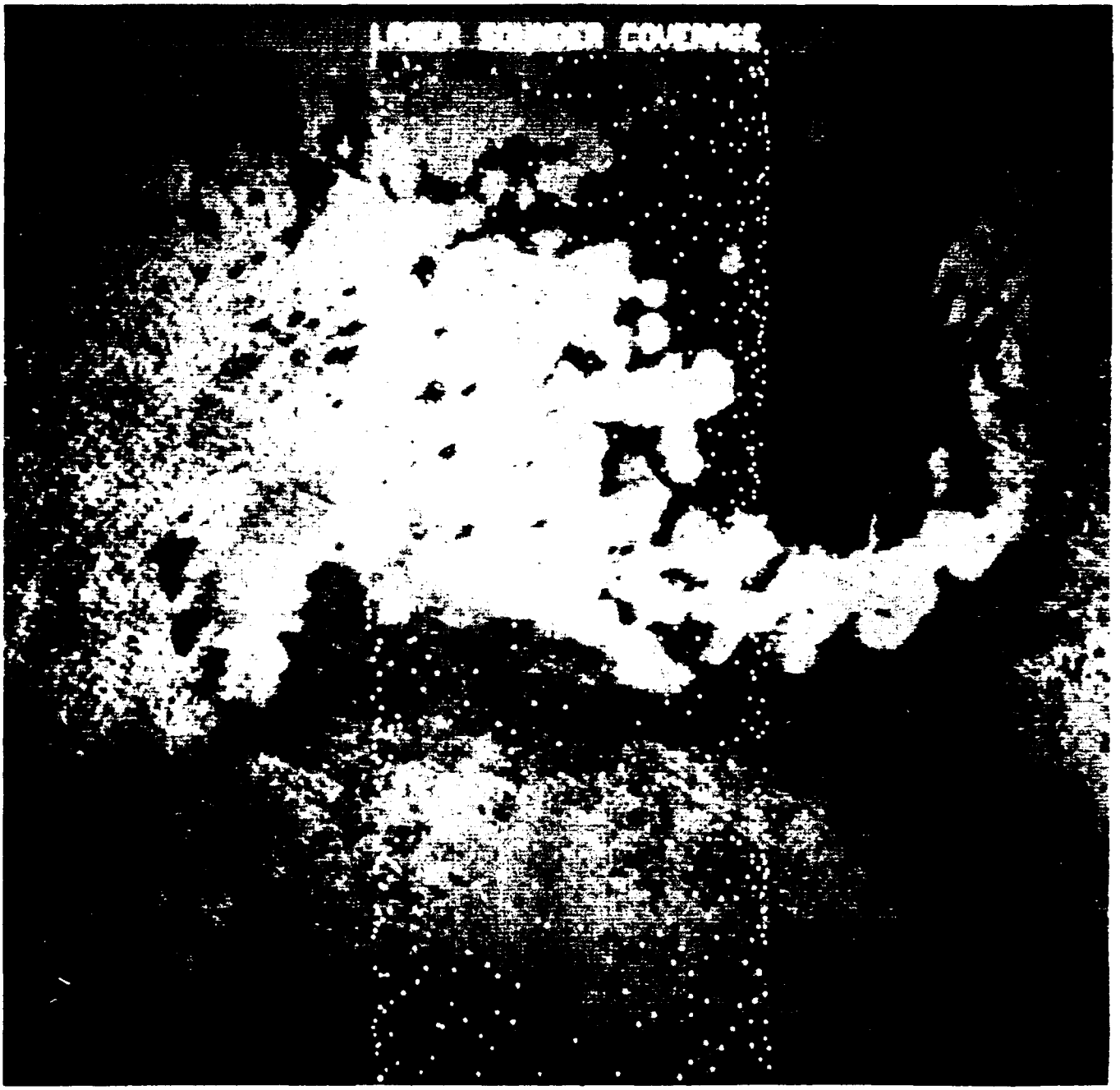

Figure 6. Image showing laser point locations registered to NS image in Key West test area. Helical scan pattern of laser can be seen.

Figure 7 NS Bands 2, 4, 5 for Panama City.

Figure 8. Corrected image demonstrates a visual improvement. The breaking waves were also corrected

Figure 9. Eastern Sambo Shoals, Key West.

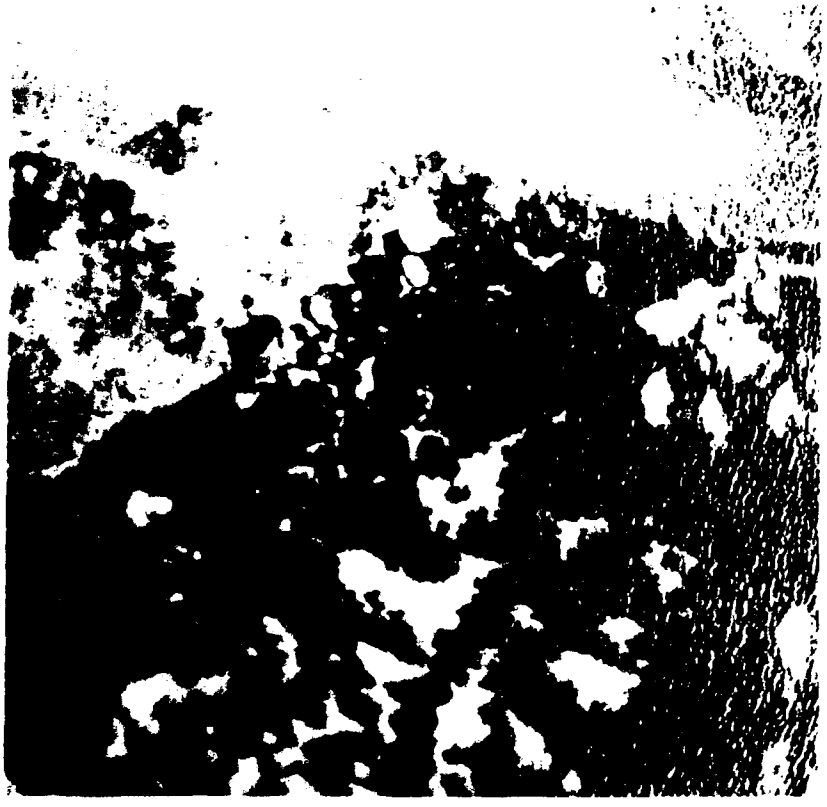

Figure 10. Bottom feature not apparent in original visible image band after glint correction

area. This is an indication that only the surface-reflected signal was removed. The details of the glint removal are shown in Appendix B.

Depth Estimate Results

The LMS and Regression models (App. B) were run extensively in the Key West area of Eastern Sambo Shoals (Fig. 6). The bathymetric ground truth was collected by NAVOCEANO in April 1987. The survey track line spacing was 25 m, with a 25-m interval between reported depth soundings. NAVOCEANO provided smooth sheets reduced from the survey data in both hard copy and computer compatible form.

The results for a comparison of LMS versus multiband regression methods are shown in Table 5. Although the LMS did relatively well in areas of constant bottom type, it did not do as well with highly varying bottom types. One reason is that the nature of the algorithm makes the coefficients adapt at different rates, depending on the model parameters and roughness of the bottom. When the bottom changes, the algorithm adapts the coefficients by the amount of error in the predicted versus the observed depth. These large error spikes contribute heavily to overall error, since the squared error is used to measure rms errors.

Tables 6 through 8 give results for the multiband model for different band combinations used in testing the model estimates against the NAVOCEANO ground truth data. The combination of bands 2 and 4 gave results similar to the five-band model. High correlation in the visible bands is the main cause, since the addition of extra channels does not add extra information. The results also show a depth dependence in the errors (Fig. 11), although the percent error is reasonably constant. Although the error in shallow water was close to 0.3 m, at or below 3 m, the errors beyond 3 m were above the 0.3-m IHO standard.

The boat sounding depths were used as control data for depth estimation from the multispectral data; the boat depth data showed better correlation with the multispectral depth data than did the laser sounder depth data. Also, more confidence could be placed in the registration of the MSS data with the boat data. The positional accuracy of the laser data was never validated. When reliable laser data becomes available and problems are resolved, more tests will be done. Plots of the MSS data versus the boat and laser sounder data are compared in Figures 12 and 13 respectively. The computed depth image for the Eastern Sambo Shoals area is shown in Figure 14.

CPU Time

Run-time results are given for a 512×512 image processed on a Digital Equipment Corporation VAX 8700 computer at NOARL (Table 9). This machine has a processing speed of approximately 6 million instructions per second (mips).

Summary

A software package that computes shallow-water depths from multispectral data combined with boat- or laser-derived soundings was developed. The best algorithms did not produce accuracies within the IHO standards of 0.3 m at depths greater than 3 m. The horizontal accuracies depend highly on the constellation of the GPS satellites, since high PDOPs give unreliable estimates. The horizontal accuracy derived from a ground control test gave accuracies of 25 m, but the PDOPs were too high to give a good control point position estimate.

High correlation in the multispectral wavebands causes difficulty in separating bottom-type effects from depth effects on the return of the signal. Since modeling the depths from the multispectral data

Table 5. Comparison of RMS error for multiband algorithms and LMS results using NAVOCEANO ground truth data.

	LMS	Multiband
Control set	1.44 m	1.01 m
Test set	1.53 m	1.07 m

Table 6. Multiband model results using NS Bands 1 through 5. Errors are in meters.

Max Depth	Regr. R^2	No. Calib.	Points Test	Mean Error	RMS Error
10	0.701	270	269	0.079	1.270
9	0.692	265	265	0.075	1.252
8	0.670	236	234	0.079	1.143
7	0.602	190	190	-0.0005	0.986
6	0.633	142	140	-0.097E-05	0.855
5	0.603	73	73	0.058	0.691
4	0.631	38	40	0.062	0.544
3	0.881	12	12	-0.954E-06	0.323

Table 7. Two channel results from multiband model using combinations of Bands 1, 2, 3 and 4. Errors are in meters.

Depth	Sensor/ Bands	R^2	(Actual-Calculated) Mean	RMS	No. Calib. Points	No. Test Points
0-3	NS/13	0.587	-0.4167E-01	0.320	12	12
	NS/14	0.843	-0.9537E-06	0.322	12	12
	NS/23	0.666	-0.8333E-01	0.311	12	12
	NS/24	0.828	-0.9537E-06	0.3227	12	12
0-4	NS/13	0.374	-0.9537E-06	0.5701	38	40
	NS/14	0.605	0.8750E-01	0.5743	38	40
	NS/23	0.170	-0.1250E-01	0.4998	38	40
	NS/24	0.488	0.5000E-01	0.5679	38	40
0-5	NS/13	0.457	0.1027E-01	0.7590	73	73
	NS/14	0.593	0.7877E-01	0.6785	73	73
	NS/23	0.264	-0.1027E-01	0.8516	73	73
	NS/24	0.484	0.7877E-01	0.7225	73	73
0-6	NS/13	0.460	-0.6429E-01	0.9790	142	140
	NS/14	0.614	-0.3929E-01	0.8368	142	140
	NS/23	0.398	-0.2143E-01	1.204	142	140
	NS/24	0.604	-0.1429E-01	0.8833	142	140
0-7	NS/13	0.430	0.7894E-02	1.168	190	190
	NS/14	0.588	-0.1053E-01	1.004	190	190
	NS/23	0.384	0.2631E-01	1.220	190	190
	NS/24	0.570	0.1579E-01	0.9943	190	190
0-8	NS/13	0.469	0.3205E-01	1.351	236	234
	NS/14	0.656	0.6624E-01	1.186	236	234
	NS/23	0.419	0.1068E-01	1.34	236	234
	NS/24	0.633	0.5555E-01	1.15	236	234
0-9	NS/13	0.502	0.6509E-01	1.459	265	265
	NS/14	0.681	0.6887E-01	1.293	265	265
	NS/23	0.420	0.4245E-01	1.485	65	265
	NS/24	0.638	0.3113E-01	1.243	265	265
0-10	NS/13	0.518	0.6227E-01	1.484	270	269
	NS/14	0.690	0.6970E-01	1.301	270	269
	NS/23	0.432	0.4740E-01	1.514	270	269
	NS/24	0.646	0.6041E-01	1.269	270	269

requires as many bands as there are cover types, more independence between bands or less cover types is necessary. Since the independence condition cannot be overcome, a reduction of cover type is more desirable. The number of cover types can be reduced by conducting the analysis over a smaller area. The problem with using a smaller area is that the number of soundings must be denser to provide adequate information to the model. The success of the system is more probable over areas with little variability in bottom cover.

The multispectral data are of considerable value alone, since the high resolution and the visibility through the water column provide a wealth of information about the nature of the coastal environment. The success of the glint-removal algorithms is valuable as a tool for "seeing" through highly glinted water surfaces. The use of common classification algorithms is useful for finding anomalies in these types of data. These tools, along with the GPS positioning data, are valuable for updating existing hydrographic charts.

In conclusion, the MIDAS system was completed for use with the ABS system. The multispectral imagery can now be processed for deriving bathymetry in clear, shallow waters down to 20 m. The system's accuracy varies with depth; for example, for water depth less than 3 m, accuracy is 0.33 m, and at a water depth of 10 m, accuracy is 1.6 m. The system may be used as is to compute bathymetric grids from multispectral data in conjunction with hydrographic boat survey data or

Table 8. Two band results using combinations of Band 5 and Bands 1 through 4. Errors are in meters.

Test Depth Residuals						
Depth	Sensor/ Bands	R^2	(Actual-Calculated) Mean	RMS	No. Calib. Points	No. Test Points
0-3	NS/35	0.574	-0.9537E-06	0.3227	12	12
	NS/45	0.756	-0.4167E-01	0.3200	12	12
0-4	NS/35	0.165	-0.9537E-06	0.5244	38	40
	NS/45	0.305	-0.1250E-01	0.5122	38	40
0-5	NS/35	0.207	-0.3767E-01	0.7935	73	73
	NS/45	0.179	-0.2397E-01	0.8111	73	73
0-6	NS/35	0.211	-0.6786E-01	1.504	142	140
	NS/45	0.311	-0.1179E-00	1.006	142	140
0-7	NS/35	0.273	-0.7896E-02	1.217	190	190
	NS/45	0.357	-0.2632E-01	1.153	190	190
0-8	NS/35	0.322	-0.1710E-01	1.424	236	234
	NS/45	0.430	-0.2351E-01	1.373	236	234
0-9	NS/35	0.285	0.3868E-01	1.651	265	265
	NS/45	0.362	-0.9444E-03	1.585	265	265
0-10	NS/35	0.281	0.1208E-01	1.671	270	269
	NS/45	0.348	-0.4648E-02	1.621	270	269

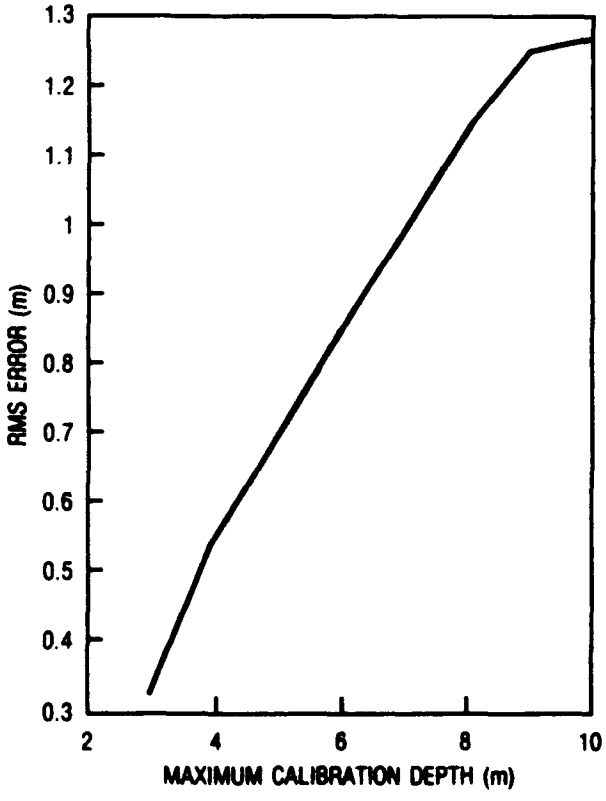

Figure 11. The rms error of depth estimates plotted against depth for multiband regression model used with boat soundings and five bands of NS data in Key West test area.

laser-derived survey data. Boat survey data were used to develop this particular system, since laser-derived depths were not as reliable.

Recommendations

In the future, better data collection systems and algorithms, along with the complete GPS constellation, will become available. This improved data collection ability will yield measured depths closer to IHO standards, for depths greater than 3 m. Also, data with less noise, better horizontal accuracy, and better ground truth, along with more knowledge about the optical parameters of the water, could give much better bathymetry estimates.

Bathymetric charts were derived using this system for the Ocean Venture '90 exercise over Isla De Vieques, Puerto Rico. Charts were developed from multispectral imagery to support amphibious assault force exercises and to determine the usefulness of such products in amphibious warfare. There are many other uses for this type of product, especially if models can be generalized to areas for which no bathymetry ground truth exists.

Since present techniques can give rms errors between 11% and 16 % of water depth, they can be

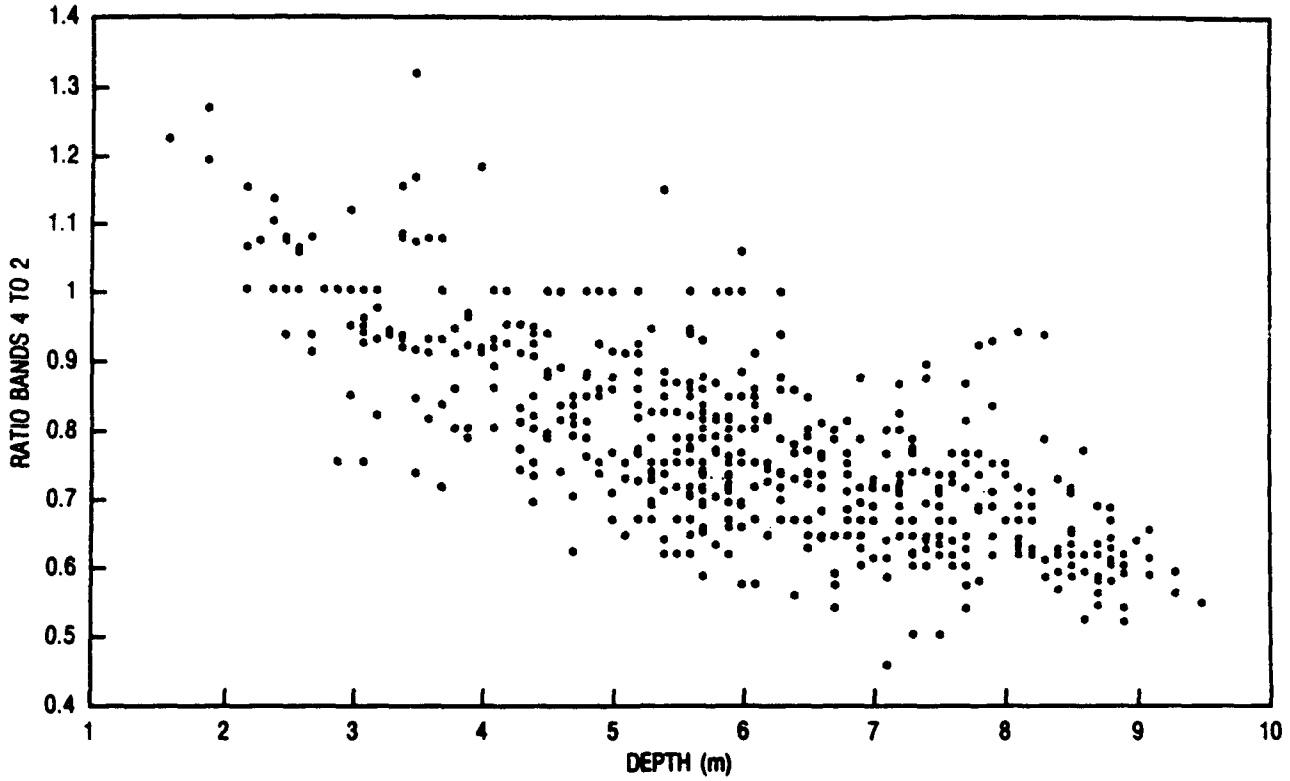

Figure 12. Plot of NS band ratio (ch. 4 to ch.2) versus depths from boat sounding data in Key West test area.

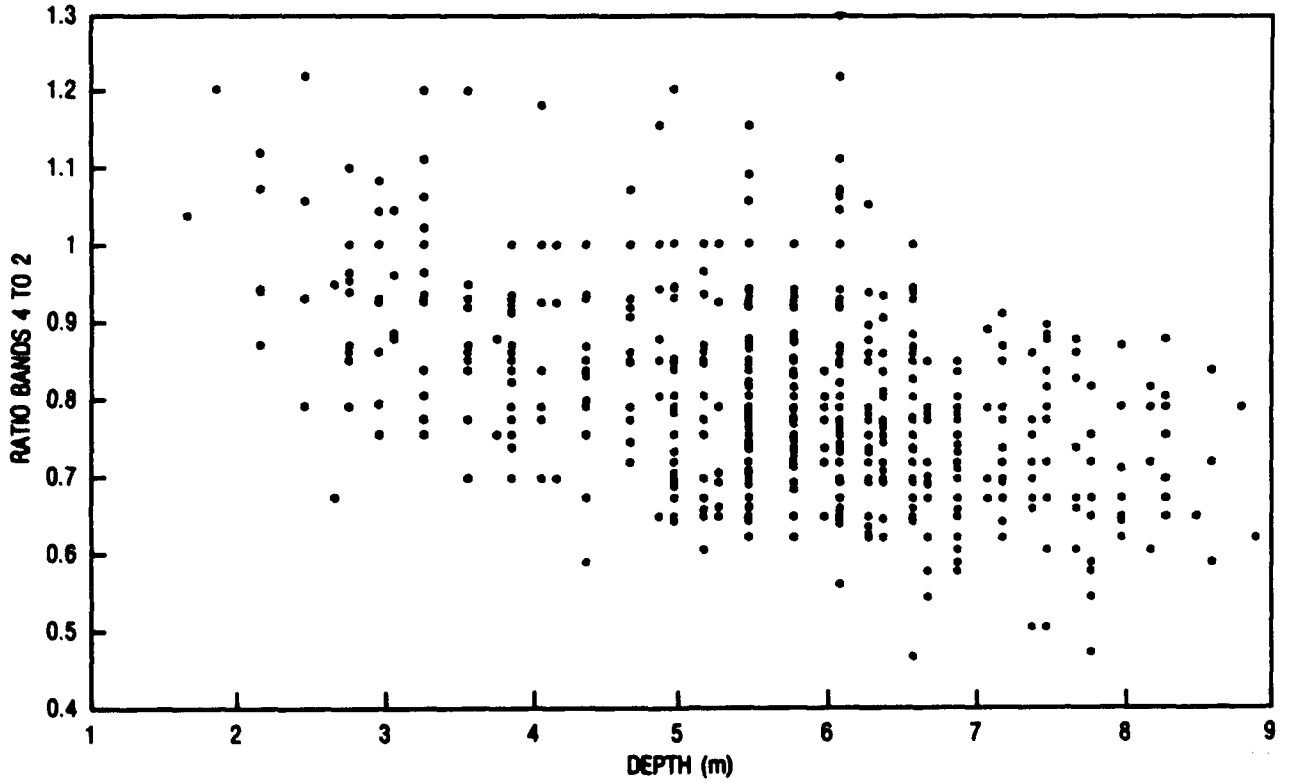

Figure 13. Plot of NS band ratio (ch. 4 to ch. 2) versus depths from laser sounder data in Key West test area.

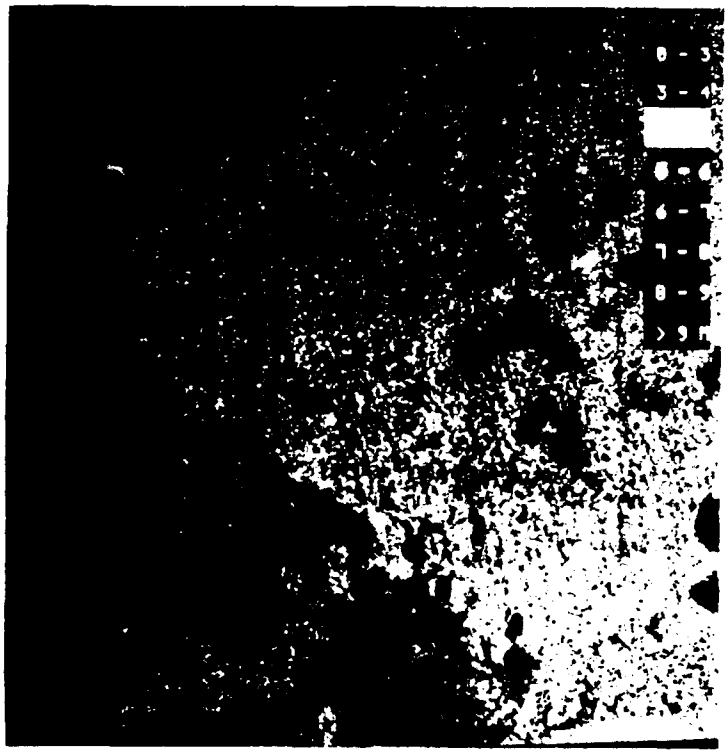

Figure 14. Depth image off northwest of Eastern Sambo Shoals area (lower right corner) Color bars show depth contour intervals in meters.

Table 9. CPU time to process a 512 × 512 image.

Module	CPU Seconds
Initialization	00:00.33
DEBLOCK, PNAV	00:11.30
GEORECT	00:58.41
GEOMATCH	00:02.84
DEEP (inc.output)	00:18.43
Total Time	01:32.41

useful in situations where relative depth (e.g., the shallowest versus deepest areas) along a coastline needs to be determined. Such products can also be used to update old charts with information on new channels, dredging, sediment deposition areas, coastline erosion, harbors, bridges, and construction. This type of information is easily available at a low cost from multispectral imagery derived depth and enhanced coastline charts.

References

Austin, R. W. (1981). Remote sensing of the diffuse attenuation coefficient of ocean water. Presented at *29th Symposium of the AGARD Electromagnetic Wave Propagation Panel on Special Topics in Optical Propagation*, Monterey, California, April.

Booker, LCDR R. W. (1986). USN, FY87-92 Hydrographic 6.3/6.4 R&D Program Brief. *HQDMA/REG*, May.

Bowditch, N. (1975). *American Practical Navigator Volume II*. Defense Mapping Agency Hydrographic/Topographic Center, Washington, DC.

Clark, R. K., T. H. Fay, C. L. Walker (1988). Bathymetry Using Thematic Mapper Imagery. *SPIE Ocean Optics IX*, Orlando, Florida, April.

Clark, R. K., T. H. Fay, C. L. Walker (1987). *A Comparison of Models for Remotely Sensed Bathymetry*. Naval Ocean Research and Development Activity, Stennis Space Center, Mississippi, NORDA Report 145.

Clark, R. K., T. H. Fay, C. L. Walker (1987). Bathymetry calculations with landsat 4 TM imagery under a generalized ratio assumption. *Applied Optics*, 26(19):4036-4038.

Compton, J. S., Commodore and Lt. Cdr M. A. Hudson (1988). New Charting Technology in Australia: The Laser Airborne Depth Sounder. *International Hydrographic Review*, Monaco, LXV(2), July.

Dowling, G. B. and M. R. Bradley (1987). *The Coastal Optical Planner Subsystem of the*

NORDA/NOO Airborne Bathymetric System: First Level Economic Feasibility Analysis. Planning Systems Inc., Slidell, Louisiana, PSI Technical Note TN-S424020.

Draper, N., and H. Smith (1981). *Applied Regression Analysis*. New York, John Wiley & Sons, 97-101.

Enabnit, D. B., L. R. Goodman, G. K. Young, and W. J. Shaughnessy (1979). *The Cost Effectiveness of Airborne Laser Hydrography*. NOAA Technical Report NOS 26. National Oceanic and Atmospheric Administration, Rockville, MD.

Hickman, G. D., M. M. Harris, D. L. Durham, and R. K. Clark (1986). The airborne bathymetric survey system. *Marine Technology Society Journal*. 20(2):5-13.

Hord, R. M. (1986). *Remote Sensing Methods and Applications*. New York, John Wiley & Sons.

Jerlov, N. G. (1968). *Optical Oceanography*. New York, Elsevier.

Kalcic, M., S. Haimbach, G. Terrie, S. Lingsch, and A. Martinez (1989). *NORDA Scanner Software Phase I Summary Report*. Naval Ocean Research and Development Activity, Stennis Space Center, Mississippi, NORDA Technical Note 417.

Kalcic, M., S. Lingsch, L. Peckinpaugh, and J. Casey. (1988) *MIDAS Users Manual and Source Code: Multispectral Image Depth Analysis System*. Naval Ocean Research and Development Activity, Stennis Space Center, Mississippi, NORDA SP 013:351:89.

Lingsch, S., M. T. Kalcic, C. L. Walker, A. B. Martinez (1989). *Application of Glint Removal Techniques to NORDA Scanner Data*. Naval Ocean Research and Development Activity, Stennis Space Center, Mississippi, NORDA Technical Note 467.

Lyzenga, David R. (1985). Shallow-water bathymetry using combined lidar and passive multispectral scanner data. *Remote Sensing*. 6(1):115-125.

Martinez, A., R. T. Joy, M. T. Kalcic, G. Terrie, and S. P. Haimbach (1988). Adaptive Estimation of Water Depth Using Multispectral Remote Sensing. *Proceedings, SPIE Ocean Optics IX*, April.

Mitchell, O. R., C. R. Myers, and W. Boyne (1977). A MAX-MIN measure for image texture analysis. *IEEE Trans. Comp*. C-26:408-414.

Motorola Inc. (1987). *Eagle Mini-Ranger Global Positioning System Receiver User's Manual*. Position Determining Systems, Arizona, Motorola Document No. 68-P29027U.

Olsen, C. (1979). Image Formation. *Proceedings of the U.S. North Atlantic Regional Workshop*, May.

Paredes, J. M. and R. E. Spero (1983). Water depth mapping from passive remote sensing data under a generalized ratio assumption. *Applied Optics*. 22(8):1134-1135.

Plass, G. N., G. W. Kattawar, and J. A. Guinn, Jr. (1976). Radiance distribution over a ruffled sea: contributions from glitter, sky, and ocean. *Applied Optics*, 15(12):3161-3165.

Polcyn, F. C. (1976). *NASA/Cousteau Ocean Bathymetry Experiment-Remote Bathymetry Using High Gain LANDSAT Data*. NASA, Goddard Space Flight Center, Greenbelt, Maryland, NASA CR-ERIM 118500-1-F.

Schanda, E. (1986). *Physical Fundamentals of Remote Sensing*. New York, Springer-Verlag.

Shifrin, K. S. (1988). *Physical Optics of Ocean Water*. New York, American Institute of Physics.

Spitzer, D., and R. Dirks (1987). Bottom influence on the reflectance of the sea. *Int. J. Remote Sensing*, 8(3):279-920.

Wells, D. (1986). *Guide to GPS Positioning*. Canadian GPS Associates. Canadian Institute of Surveying and Mapping, Ottawa, Ontario, Canada.

Widrow, B. and S. D. Stearns (1985). *Adaptive Signal Processing*. Prentice-Hall, Englewood Cliffs, N.J.

Appendix A

NOARL Scanner System and Specifications

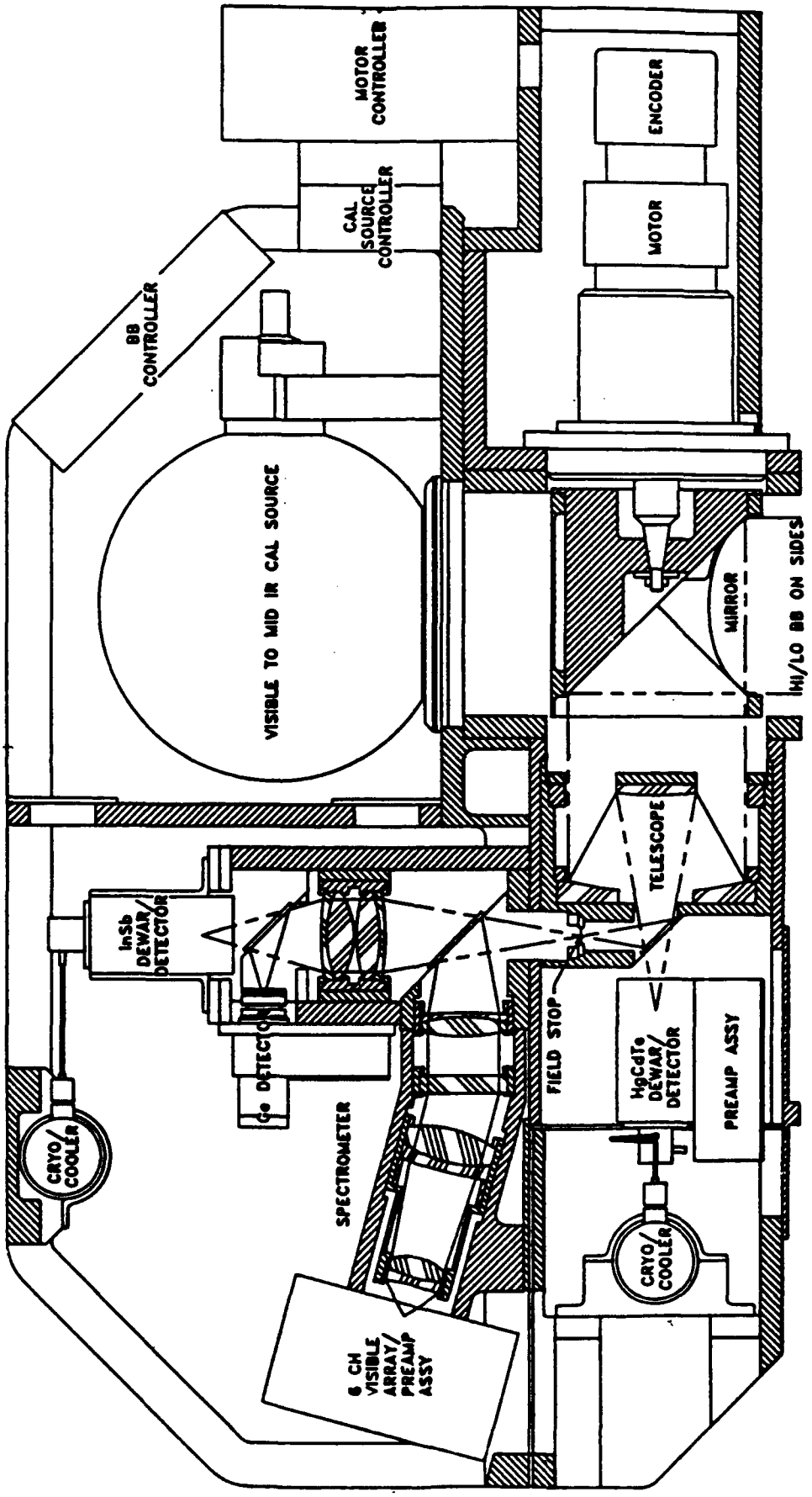

Figure A-1. Schematic diagram of NOARL scanner.

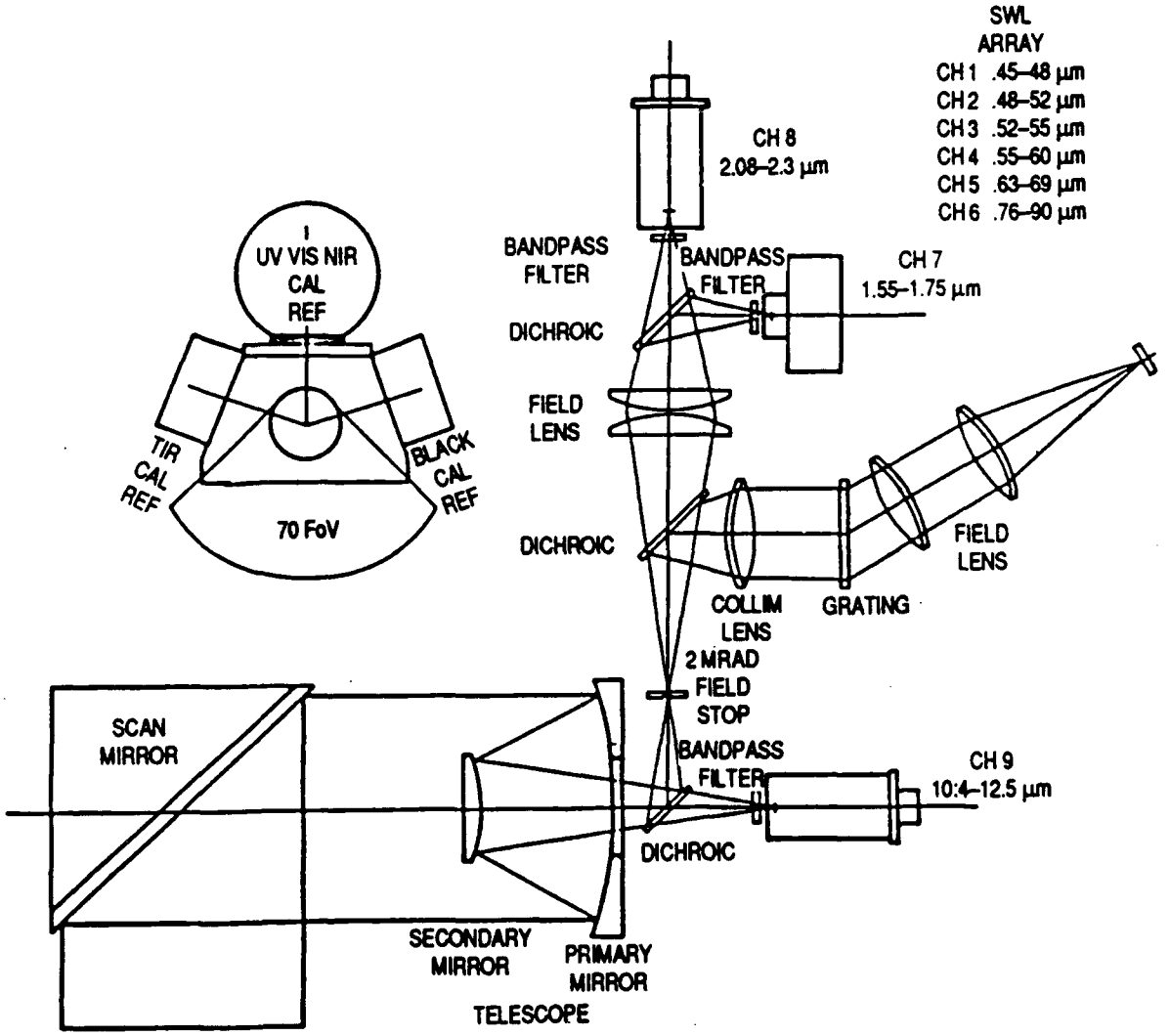

Figure A-2. Schematic diagram of NOARL scanner optical paths.

SPECIFICATIONS:

9 CHANNELS
- 6 VISIBLE
- 3 IR

SCAN MIRROR
- ROTATING OPTICAL FLAT
- 10.16 CM DIAMETER
- ROTATION RANGE: 30 TO 165 RPS

DIGITAL ELECTRONICS
- 3142 RESOLUTION ELEMENTS PER SCAN
- 628 VIDEO RESOLUTION ELEMENTS PER SCAN
- DIGITIZATION LEVEL 8 BITS

CALIBRATION SOURCES
- 2 BLACK BODIES AND A FIELD FILLING INTEGRATING SPHERE FOR EACH MIRROR REVOLUTION
- SCANNER DATA WILL BE CALIBRATED IN A POST-PROCESSING MODE WITH LASER SOUNDINGS

SYSTEM CHARACTERISTICS
- WEIGHT—275 LB
- POWER
- 28 VDC

Figure A-3. NOARL scanner specifications.

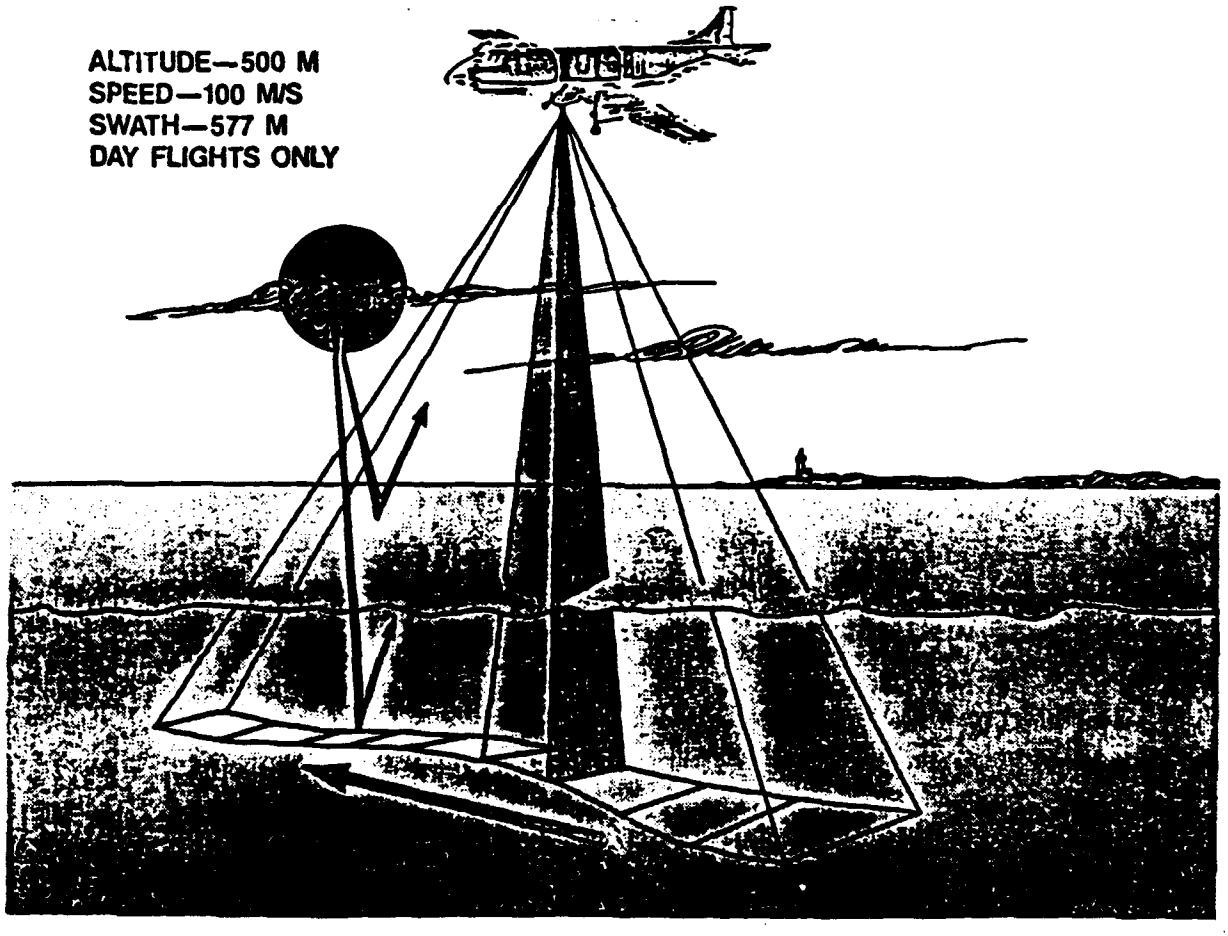

Figure A-4. NOARL scanner operational scenario.

Appendix B

Algorithms and Techniques

POSITIONING

The Global Positioning System (GPS) provides latitude, longitude, and heading approximately every second. A scan rate of 100 scan lines per second yields a positional update every hundred lines. Positions are linearly interpolated between updates as a function of time to produce latitudes and longitudes for individual scanlines.

GEOMETRIC CORRECTIONS

Corrections for roll, pitch, yaw and scan angle distortion are applied to the GPS derived latitudes and longitudes to derive positioning for each pixel.

The first step corrects for scan angle distortion. As the distance from nadir increases, the pixel footprint size increases. The distance to the center of each pixel relative to nadir is computed by

$$Dx = \text{TAN}((N * IFOV) + IFOV/2) * Alt, \quad (1)$$

where

N = Pixel number (negative left of nadir, positive right of nadir);

IFOV = Instantaneous field of view (0.002 Radians);

Alt = Aircraft altitude (m);

Dx = Distance from nadir to center of pixel N (m).

If the scanner is not roll compensated, the roll correction is applied and the equation becomes

$$Dx = \text{TAN}((N * IFOV) + (IFOV/2) - ROLL) * Alt. \quad (2)$$

A positive roll angle, or right bank roll, translates the scanline to the left, and a negative roll translates the line to the right.

The pitch correction, Dy, translates the entire line forward or backward by the ground distance traveled when the scanner rotates about the angle of pitch.

$$Dy = Alt * \text{TAN}(PITCH) \quad (3)$$

The offsets are rotated by the true heading relative to the geographic coordinate system. The true heading is computed from the heading received from the GPS and the drift or yaw received from the INS. The GPS heading is computed from point to point locations. The drift angle is then defined as the deviation of the aircraft's longitudinal axis from the GPS heading. A positive drift means the nose of the aircraft points left. The true heading is given by:

$$\Theta = Heading - Drift \quad (4)$$

Each pixel is then multiplied by a rotation matrix, equation 5, and, offsets Dx' and Dy' in meters are computed for the pixel's distance from the center position.

$$\begin{bmatrix} Dx \\ Dy \end{bmatrix} \cdot \begin{bmatrix} \cos\Theta & \sin\Theta \\ -\sin\Theta & \cos\Theta \end{bmatrix} = \begin{bmatrix} Dx' \\ Dy' \end{bmatrix} \quad (5)$$

The latitude and longitude are computed using conversion formulas from Bowditch (1975).

Degrees / Meter of Latitude
= 111132.09 - 566.05 * COS(2 * Latitude) +
1.2 * COS(4 * Latitude) - 0.002 * COS(6 * Latitude)
Degrees / Meter of Longitude
=111415.13 * COS(Latitude) - 94.55 * COS(3 * Latitude) +
0.12 * COS(5 * Latitude)

SUBAREA DETERMINATION AND MAPPING EQUATIONS

Each continuous flight line is divided into subareas for processing. Each subarea covers approximately a 600 x 500 m area. The first step computes the boundaries of the subarea. Distances AB and DE in Figure B-1 are computed by

$$\text{Alt} * \text{TAN}((\text{Pix}/2 - \text{Ste}) * \text{IFOV}), \tag{6}$$

where

Pix = Number of pixels in scanline.
Ste = Starting element number.

Distances AC and DF are computed by

$$\text{Alt} * \text{TAN}((\text{Ene} - \text{Pix}/2) * \text{IFOV}), \tag{7}$$

where

Ene = ending element number.

Variables Ste and Ene are region-of-interest boundaries, which define the area to be processed. Portions of the image may not be processed due to sun glint/glare or other environmental factors.

Once these distances are computed, B and C are rotated about A, and E and F are rotated about D by the heading. B', C', E', and F' become the subarea corner points. Approximately 512 scanlines are processed in a subarea; hence, D is about 512 lines from A. This size depends on the scan rate and the aircraft's speed. A and D are known geographic locations that have been corrected for aircraft attitude. Geographic locations are computed for the corner points. The top boundary of the subarea will become the lower boundary of the subsequent subarea processed.

Six control points are defined as shown in Figure B-1 (A, B', C', D, E', and F'). Additional control points are added by sampling every 50th scanline. The distance of the center pixel from the center of the subarea is computed by using the Law of Cosines. Twenty control points along the scanline are geometrically corrected as in the previous step, giving roughly 200 equally spaced control points within the subarea. Once all the control points are computed, mapping coefficients are computed using a second order polynomial. The following equation converts latitude and longitude to line and element:

$$\text{Line} = B_1 + B_2\ \text{Lat} + B_3\ \text{Lon} + B_4\ \text{Lat}^2 + B_5\ \text{Lon}^2 + B_6\ \text{Lat Lon}, \tag{8}$$

$$\text{Elem} = C_1 + C_2\ \text{Lat} + C_3\ \text{Lon} + C_4\ \text{Lat}^2 + C_5\ \text{Lon}^2 + C_6\ \text{Lat Lon}, \tag{9}$$

where

B_n = Line coefficients,

C_n = Element coefficients.

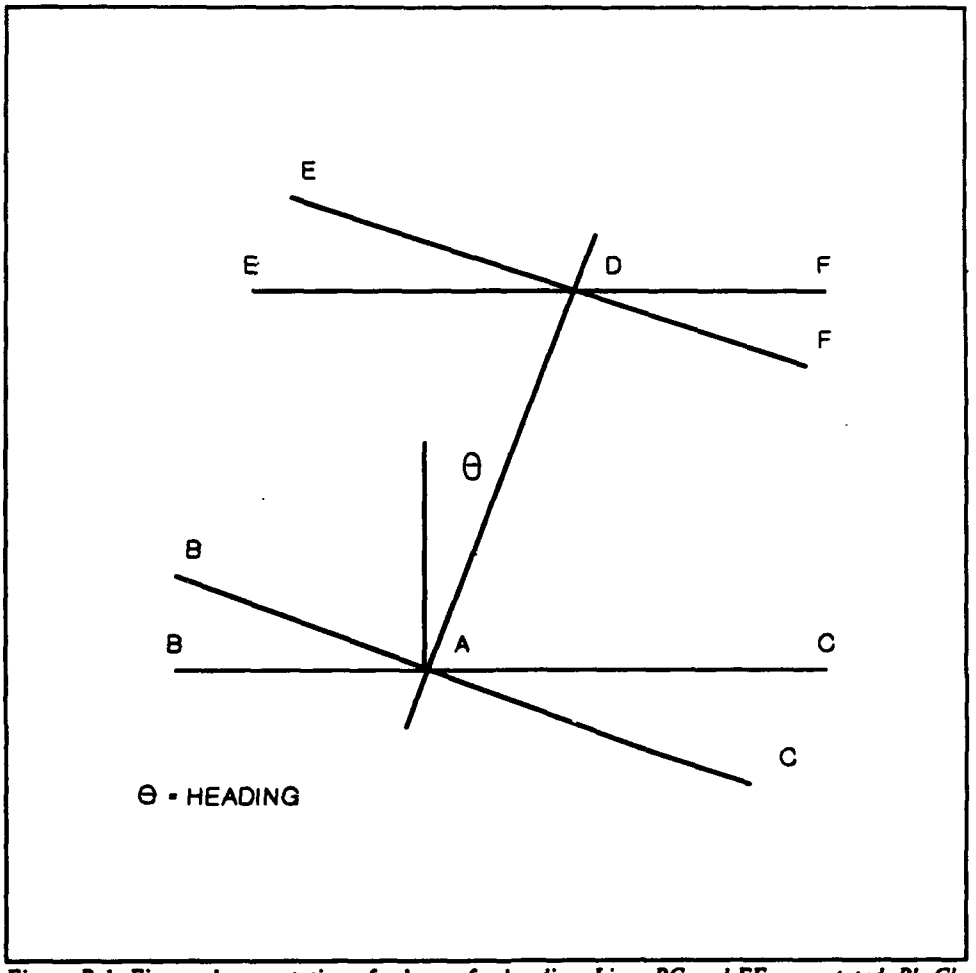

Figure B-1. Figure shows rotation of subarea for heading. Lines BC and EF are rotated, B', C', E', and F' become corner boundaries of subarea.

Each pixel goes through the transformation for aircraft attitude and is mapped to the geographic grid by equations 8 and 9. Data gaps occur for the following reasons. As the distance from nadir increases, the distance between the center of pixels increases, i.e., at an altitude of 500 m the distance between pixels becomes 1.7 m at the farthest off-nadir position. When transformed to a 1-m grid, this effect causes a gap on the vertical axis. Gaps in the horizontal axis occur depending on the sample rate, air speed, and changes in the aircraft's attitude. Nearest neighbor interpolation is used to fill in these gaps. If the vacant cell does not have an adjacent neighbor, no value is placed in that cell and no depth is computed for that position.

Equations 8 and 9 can be used to register any external source of soundings to the image. An advantage to this method is any data set can be registered to the multispectral image regardless of the source or the time collected. At the same time the coefficients are generated, coefficients for the inverse problem are computed (i.e., given line and element compute latitude and longitude). This is useful for later reference and mosiacking subareas to produce a complete bathymetric chart.

GLINT REMOVAL

Passive multispectral data collected over water are subject to both specular and diffuse reflection off the surface of the water. This component of the signal appears as glint or glare at the sea surface and must be removed from the signal for bathymetry estimators to be effective.

Several authors (Lyzenga, 1985; Spitzer, 1987) have reported the signal in the near infrared (IR) band is useful in determining the magnitude of surface reflection. Transmittance of visible wavelengths is good, but a significant absorption band occurs in the near-IR band (750-760 nm) (Jerlov, 1968). As a result, while surface reflection and atmospheric returns are common to all bands, the light reflected from the water column and the bottom is mostly light in the visible wavelengths (450-690 nm).

Lyzenga (1985) proposes a method that exploits the spectral characteristics of sun glint to derive a correction for surface reflection. He assumes a linear relationship between the glint in the visible and IR channels. This results in a glint correction for visible band i based on IR channel j of the form,

$$\Delta Y_i = A(Y_j - \bar{Y}_j). \tag{10}$$

The corrected visible band signal is given by

$$\hat{Y}_i = Y_i - \Delta Y_i, \tag{11}$$

where

Y_i = Raw signal for visible band,

$\bar{Y}_j$ = Average IR signal in a non-glinted deep water region,

σ_{ij} = Covariance of the visible and the near IR bands computed in a deep water region,

σ_{jj} = Variance of the near-IR band,

$A = \sigma_{ij} / \sigma_{jj}$.

Lyzenga suggests the method is valid when the correlation coefficient is greater than 0.90.

Two observations motivate modifications and extensions of Lyzenga's method. A linear model may not accurately represent the relationship between the output of the scanner sensors. Figure B-2 is a typical scatter plot of raw data from the NOARL scanner channel 6 versus channel 4. Motivation for a higher order model is clearly given in the nonlinear relationship between the channels. Second, in shallow water, the indiscriminate application of Lyzenga's method has been seen to remove prominent features such as sandbars. The solution proposed here is to identify and mask the glint-free areas in the image and to process only those areas with glint.

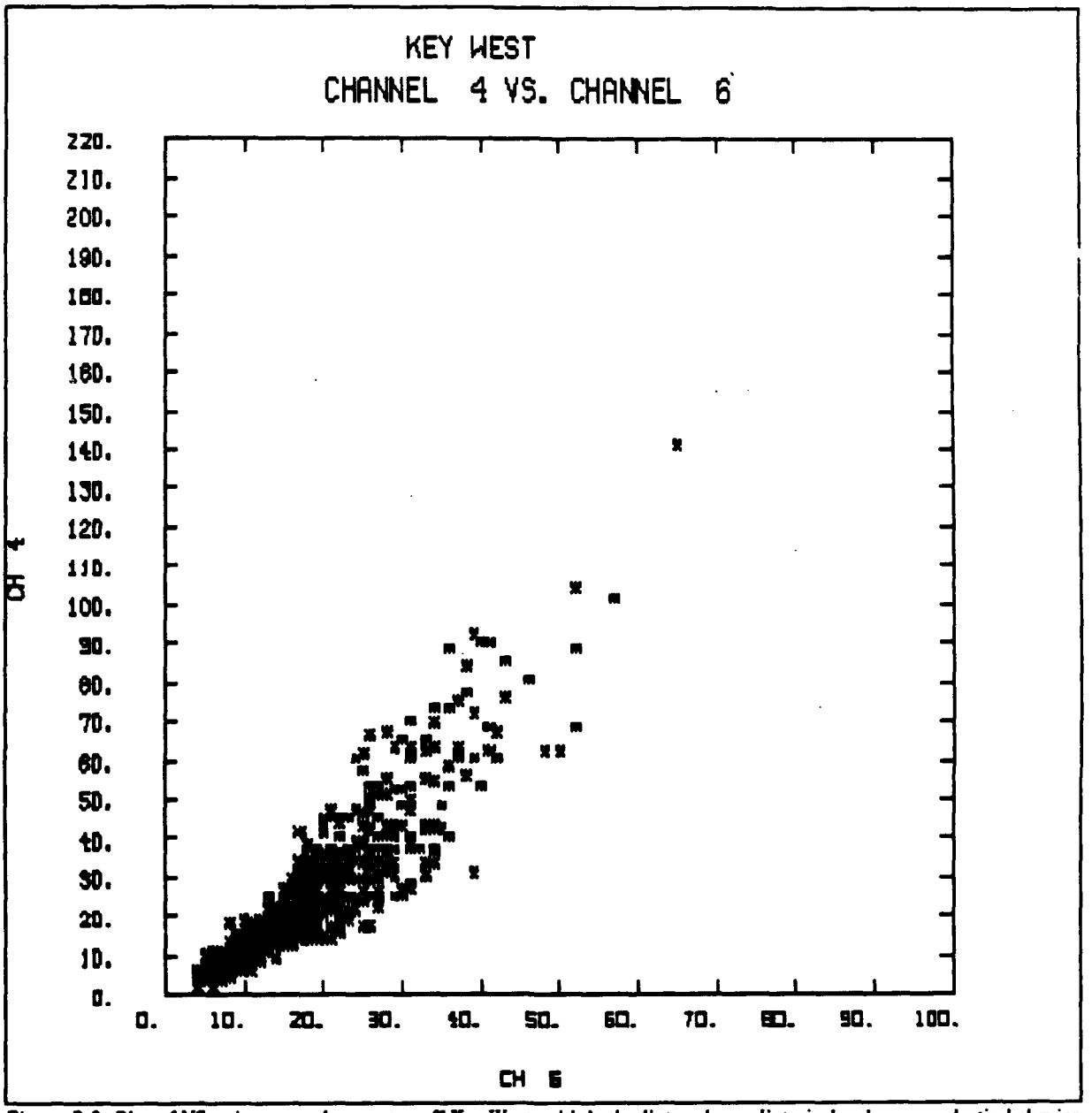

Figure B-2. Plot of NS points over deep water off Key West, with both glint and nonglint pixels, shows quadratic behavior of Band 4 versus 6.

DEEP WATER STATISTICS

The procedure for glint removal first involves preprocessing a deep water region containing both glint and nonglint. A deep-water region is chosen to assure that the signal in the visible bands is independent of bottom reflection. Since the IR does not penetrate the water column, the covariance in the IR and visible channels over deep-water is assumed to be due to glint.

Glint-contaminated regions exhibit a large pixel-to-pixel variance, and nonglint regions, a smaller variance. This variability is clearly seen in Figures B-3 and B-4, which show a typical signal cross section of a deep-water region in the near IR band and the corresponding image. Using this property, a nonglint area within the deep-water region is found and the averages Y_j and Y^2_j are computed.

A mask is produced to insure that only areas with glint are processed and that such features as land, nonglint areas, and sandbars are not altered.

The near-IR band 6 is used to distinguish land and water. A threshold is selected manually. An area in the flight line is chosen that contains both land and water. By highlighting pixels in the near IR from 0 to 255 successively, a maximum water value is obtained. Ideally, IR band 7 could be expected to distinguish surface-subsurface reflections better than band 6. However, band 7 was excessively noisy and failed to sufficiently resolve the land-water boundary.

The IR channel is also used to distinguish between possible glint and nonglint pixels. Over water, the near-IR band is assumed to consist almost entirely of surface reflection. Thus, a strong return is an indication of glint in a pixel.

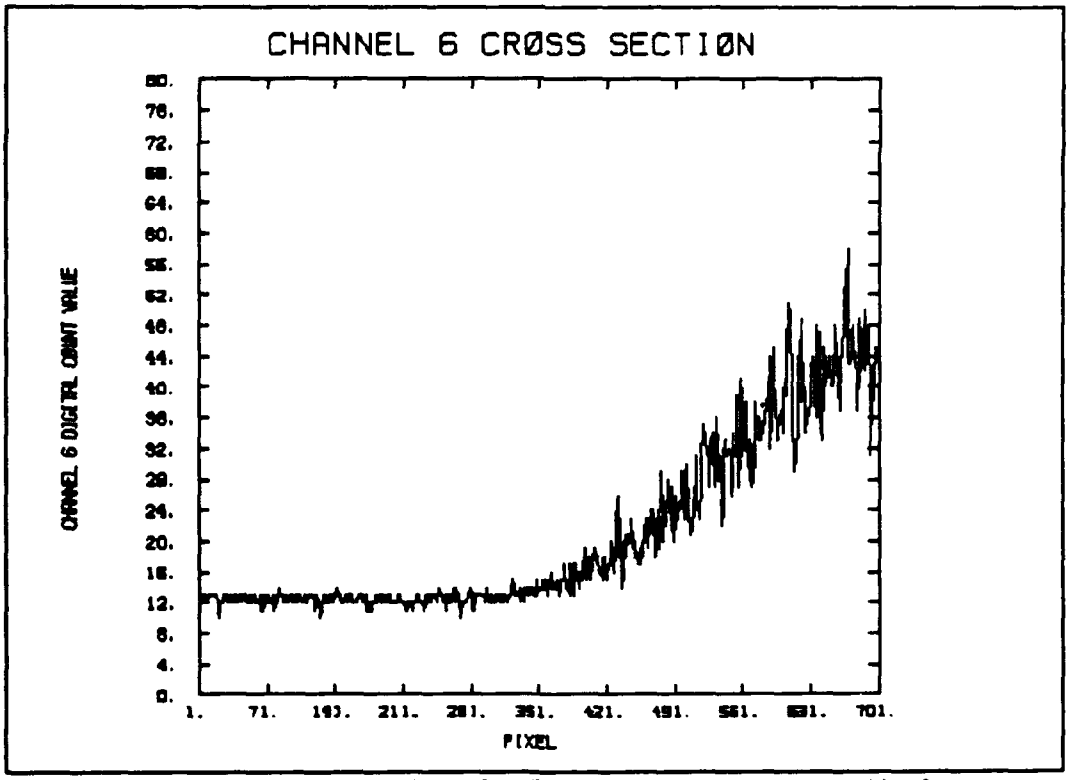

Figure B-3. Channel 6 cross section for line A-B in Figure 5 below, showing the transition from a nonglinted region to a glinted region.

Figure B-4. NS near-IR band (700-900 nm). Signal over shoals and sandbars showing tone, whereas the signal due to reflection demonstrates texture.

QUADRATIC GLINT CORRECTION

The method discussed here is a variation of Lyzenga's method, with the inclusion of a squared term in the model. The glint correction for the visible-band i based on the IR-band j takes the form,

$$\Delta Y_i = A(Y_j - \bar{Y}_j) + B(Y^2_j - \bar{Y}^2_j). \quad (12)$$

The corrected visible-band signal is given by

$$\hat{Y}_i = Y_i - \Delta Y_i, \quad (13)$$

where

Y_i = Raw signal for visible band,

Y_j = Raw signal for near-IR band,

$\bar{Y}_j$ = Average IR signal in a nonglint deep-water region,

$\bar{Y}^2_j$ = Average IR signal squared in a nonglint deep-water region, and

A, B = Regression coefficients.

Application of this model requires the identification of suitable non-glint deep water regions over which the averages Y_j and Y^2_j are computed. To compute the regression coefficients, each of the five visible

bands is regressed against the near-IR band. The region where the coefficients are computed requires a deep-water region containing both glint and nonglint.

DEPTH ESTIMATION REGRESSION MODEL ESTIMATION

Current depth algorithms are based on the functional form of the single-band radiance model (Clark et al.,1987). Statistical regression techniques are used to determine the unknown parameters using water depths known at a few pixel locations in the multispectral image. Single- and dual-band ratio models are very sensitive to changes in bottom reflectance and water clarity. Multiband algorithms in which the radiance and bottom reflectance are functions of the wavelength can be used to minimize difficulties encountered due to changes in the bottom reflectance and water attenuation. A development of the multiband model from the single-band radiance equation is presented here.

The single-band radiance equation, where total radiance from the water, L_i, for a single bandwidth (i), is written as

$$L_i = L_{\infty i} + s_i r_i \exp[-f k_i z], \tag{14}$$

where

$L_{\infty i}$ = radiance from deep water;

s_i = a function of transmittance of the air and water surface, surface refraction and solar irradiance;

r_i = bottom reflectance;

k_i = effective attenuation coefficient of the water;

f = geometric factor to account for the pathlength through the water;

z = water depth;

i = 1,2...n;

n = number of spectral bandwidths.

There have been several implementations of this model (Clark et al.,1987; Paredes and Spero,1983). Some implementations require classifying the data into bottom cover types or knowledge of optical parameters. Other implementations use band ratios and combinations of bands. Ratios work rather well if they are constant for all bottom types in the area of interest. The ratio method was outlined by Polcyn et al.(1976) and elaborated by Lyzenga (1985). The generalized band ratio algorithm has been found to give the best results as discussed by Clark et al. (1988). A brief summary of the method is given here. Equation (14) is usually linearized and solved for z to yield

$$z = (1/fk_i)\,(\ln[r_i] - X_i), \tag{15}$$

where $X_i = \ln[(L_i - L_{\infty i})/s_i]$. Equation (2) can be reparameterized with

$b_{0i} = (1/fk_i)\,(\ln[r_i])$,

$b_{1i} = -(1/fk_i)$

and

$$X_{oi} = 1 \quad .$$

The depth, z, for one channel, can then be expressed in matrix notation as

$$z = \mathbf{b}'\mathbf{x},$$

where **b'** is the transpose of the vector **b**. The vector **b** contains the weights b_0 and b_1. The vector **x** contains [1 , x].

For n bandwidths, the depth z can be expressed as a weighted sum of single-band terms as follows

$$z = w_1 b_1 x_1 + w_2 b_2 x_2 + \ldots + w_n b_n x_n,$$

where the **b** and **x** vectors are defined as above for each band, and the w's are weights whose sum equals 1. In matrix form, this equation can be written as

$$z = \mathbf{w}'\mathbf{B}'\mathbf{x}, \tag{16}$$

where **w** is a vector of n+1 weights, **B** is a diagonal matrix of weights where b_0 is a constant term derived from the sum of constant terms for each band, and **x** is a n+1 vector with $x_0 = 1$. The motivation behind the summation of constant terms (Paredes and Spero, 1983), is discussed here.

For m bottom cover types, and n bandwidths such that m = n, Paredes and Spero have shown that a vector **c** of length n exists, such that

$$\mathbf{c}'\mathbf{A} = \mathbf{1},$$

where **1** is a 1's vector of length n and **A** is defined as the n by m matrix,

$$\mathbf{A} = \begin{bmatrix} \ln r_{11} & \ldots & \ln r_{1m} \\ \ln r_{21} & \ldots & \ln r_{2m} \\ . & \ldots & . \\ . & \ldots & \ln r_{nm} \end{bmatrix}.$$

Each element of **A** is the logarithm of the bottom reflectance term for the nth channel and the mth bottom type. As long as the number of bottom types, m, is not greater than the number of channels, n, a solution for **c** can be found. Spero and Paredes show that for m=n bottom types, the weights w_i can be written

$$w_i = c_i k_i / \mathbf{c}'\mathbf{k} \; .$$

Equation 16, can be written as

$$z = \mathbf{w}'\mathbf{b}_0 + \mathbf{w}'\mathbf{b}_1\mathbf{x},$$

where

$$\mathbf{w}'\mathbf{b}_0 = (1/f)[\mathbf{c}'\mathbf{k}]^{-1} * \mathbf{c}'\mathbf{A}.$$

Since **c'A** is **1**, the bottom reflectance term goes away, and only the sum of constant terms remains. The multiband depth model can thus be expressed, independently of bottom type reflectance, as the linear regression model

$$z = \beta X + \varepsilon,$$

where β is the vector **w'B** of coefficients derived from the least-squares solution of equation 16, **X** is the vector of reflectances, and ε is the error.

Results from comparison of the multiband model to the single-band and dual-band ratio models indicate that the multiband generalized ratio technique gives superior results and is computationally efficient as well.

THE LMS ALGORITHM

Another approach taken is an adaptive fitting technique, often used in linear systems theory, called the LMS algorithm (Widrow, 1985).

Depths are estimated by

$$\acute{z} = \mathbf{w'x},$$

where $\acute{z}$ = estimated depth;

w = vector of weights, (w' is transpose);

x = vector of reflectance values.

The error at each point is given by

$$e = z - \acute{z}.$$

The weights are computed at each known depth, as follows:

$$w_{k+1} = w_k + 2\mu e_k x_k,$$

where

w_k = weight for k^{th} point;

μ = constant chosen for stability and rate of convergence;

e_k = error for the k^{th} point;

x_k = input value for the k^{th} point.

For more than one bandwidth, the equation may be expressed in matrix notation,

$$\mathbf{w}_{k+1} = \mathbf{w}_k + 2\mu e \mathbf{x},$$

where w_k is a vector of weights for each band, and x is a vector of reflectances in each band. Optionally, the x's may be ratios, and a vector of ones can also be included to add stability.

Computing the weights is quite simple and does not require much computation time. Preliminary results have shown that this technique can produce more accurate results than the use of a deterministic model.

Appendix C

Depth File Format

DEPTH DATA FILE FORMAT

A. File Name

DISK$SCANNER:[MIDAS.DATA.Mnn]TnnFnn.DEP where:
Mnn = The survey mission number (ie., M12)
Tnn = The tape number (ie., T24)
Fnn = The file number (ie., F02)

B. Usage

This file is the end product of the Multispectral Image Depth Analysis System (MIDAS). This file contains all the necessary information needed to generate a navigation chart for a specified survey area.

C. File Structure

The DEPTH data file is a variable-length, random-access, block-structured file. It contains a main header, which describes general information about the data an survey area. All depth data are stored via linked list subarea headers, which contain information about the subarea and a pointer to the first block of the packed depth data for the subarea. Refer to the next page for a description of a typical MIDAS Depth Data File format.

D. Record Structure

There are three primary record types in the MIDAS Depth Data File: The Main Header, The Sub-Area Headers, and the Packed Depth Data. Refer to the following pages for detailed descriptions of each record structure.

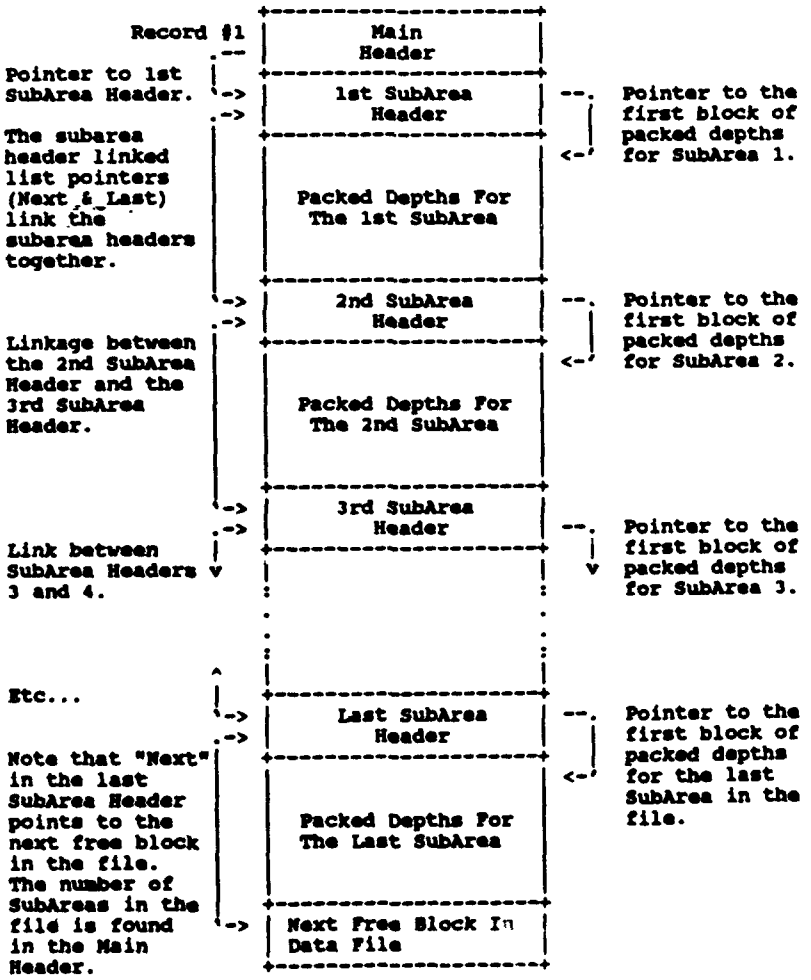

E. Main Header

Record Type: Main Header (For MIDAS Version #1)
Record Access: Block I/O (suggest ELTRAN)
Record Structure: Fixed length formatted (1024) byte) block.

Of the 1024 total bytes, 409 bytes are used with 615 bytes reserved for expansion. The Version Number (Vers) of the file at offset 4 defines what record structures to use when reading the depth file. At the time this documentation was written there was only one format (Vers 1 format). This variable should be used by the software to keep the software upward compatible. The contents of the Main Header block(s) are as follows:

Offset (bytes)	Name	Size (bytes)	Date Type	Description
0	Ident	4	CHAR	File type identification code 'DEEP'
4	Vers	4	LONG	Version number of creating software
8	SunAOf	4	LONG	Offset to first subarea
12	NoSubA	4	LONG	Number of subareas in the file
16	Mission	4	LONG	Mission number
20	Tape	4	LONG	Tape number
24	File	4	LONG	Number of file on the tape
28	Resoln	4	REAL	Resolution of the data (in meters)
32	MinLat	8	DBLE	Minimum latitude value in this file
40	MinLon	8	DBLE	Minimum longitude value in this file
48	MaxLat	8	DBLE	Maximum latitude value in this file
56	MaxLon	8	DBLE	Maximum longitude value in this file
64	Date	9	CHAR	Date of survey
73	Area	80	CHAR	Name of the area covered
153	Coment	255	CHAR	Additional comments (of any type)
408	IsQuad	1	FLAG	Flag indicating if quadratic

Data Type	Size (bytes)	VAX Fortran 77 Equivalent
CHAR	4	Character * 4
CHAR	80	Character * 80
DBLE	8	Real * 8
DBLE	32	Real * 8 array of 4
FLAG	1	Logical * 1 (.true. or .false.)
LONG	4	Integer * 4
REAL	4	Real * 4

F. SubArea Header

Record Type: SubArea Header (for MIDAS Version #1)
Record Access: Block I/O (suggest ELTRAN)
Record Structure: Fixed length formatted (512 byte) block.

Of the 512 total bytes, 192 bytes are used with 320 bytes reserved for expansion. The contents of the Subarea Header Block are as follows:

Offset (bytes)	Name	Size (bytes)	Date Type	Description
0	Next	4	LONG	Block number of next subarea header
4	Last	4	LONG	Block number of last subarea header
8	DephOf	4	LONG	Starting block number of depth data
12	NumScn	4	LONG	Number of scanNumScn in subarea
16	NumElm	4	LONG	Number of elements in subarea
20	BgnCov	4	LONG	Beginning HALS coverage element
24	EndCov	4	LONG	Ending HALS coverage element
28	SbALat	32	DBLE	Corner Latitudes for subarea
60	SbAlon	32	DBLE	Corner longitude for subarea
92	LinCof	48	DBLE	The scanline mapping coefficients
140	ElmCof	48	DBLE	The elements mapping coefficients
188	SbArea	4	LONG	The physical Subarea number

Data Type	Size (bytes)	VAX FORTRAN 77 Equivalent
CHAR	4	Character * 4
CHAR	80	Character * 80
DBLE	8	Real * 8
DBLE	32	Real * 8 array of 4
FLAG	1	Logical * 1 (.true. or .false.)
LONG	4	Integer * 4
REAL	4	Real * 4

G. Packed Depth Format

Record Type: Packed Depth Data (for MIDAS Version #1)

Record Access: Block I/O (suggest MIDAS Pack/Unpack Routines)

Record Structure: Scaled decimal (byte) data packed into a contiguous set of (512 byte blocks.

The last block in the set is padded with ASCII nulls.

Example of 511 byte records packed into 512 byte blocks:

	BYTE #	BYTE #	...	BYTE #	BYTE #	BYTE #
BLOCK	1	2	...	510	511	512
1	1, 1	2, 1	...	510, 1	511, 1	1, 2
2	2, 2	3, 2	...	511, 2	1, 3	2, 3
3	3, 3	4, 3	...	1, 4	2, 4	3, 4
...	...	...	...	...	...	...
510	510, 510	511, 510	...	508, 511	509, 511	510, 511
511	511, 511	1, 512	...	509, 512	510, 512	511, 512
512	1, 513	2, 513	...	510, 513	511, 513	1, 514
513	2, 514	3, 514	...	511, 514	<BLANK>	<BLANK>
ELEMENT, SCANLINE		**Each block represents (depth X 10) stored in a single byte at the specified Element and Scanline.**				

This example shows the typical storage of the packed depth values for a 511 element by 514 scanline subarea. There are no extra characters (such as <CR><LF>) stored in the packed data. The pack and UnPack routines use the number of elements and number of scanlines stored in the subarea header to pack and unpack the data. Depth time 10 values are stored in bytes. Valid depths are 0.1 - 20.0 meters stored as 1-200 in the file. A zero (0) represents a land value, and a 255 represents an invalid data point. The last block written will be added with binary zero (0) or ASCII null.

Distribution List

Applied Physics Laboratory
Johns Hopkins University
Johns Hopkins Road
Laurel MD 20707

Applied Physics Laboratory
University of Washington
1013 NE 40th St.
Seattle WA 98105

Applied Research Laboratory
Pennsylvania State University
P.O. Box 30
State College PA 16801

Applied Research Laboratory
University of Texas at Austin
P.O. Box 8029
Austin TX 78713-8029

Assistant Secretary of the Navy
Research, Development & Acquisition
Navy Department
Washington DC 20350-1000

Chief of Naval Operations
Navy Department
Washington DC 20350-2000
Attn: OP-71
OP-987

Chief of Naval Operations
Oceanographer of the Navy
U.S. Naval Observatory
34th & Massachusetts Ave. NW
Washington DC 20392-1800
Attn: OP-096
OP-0961B

David W. Taylor Naval Research Center
Bethesda MD 20084-5000
Attn: Commander

Defense Mapping Agency
Systems Center
8613 Lee Hwy.
Fairfax VA 22031-2138
Attn: Director
Code SGWN
SGE, Kevin Brown

Fleet Antisub Warfare Tng Ctr-Atl
Naval Station
Norfolk VA 23511-6495
Attn: Commanding Officer

Fleet Numerical Oceanography Center
Monterey CA 93943-5005
Attn: Commanding Officer

National Ocean Data Center
1825 Connecticut Ave., NW
Universal Bldg. South, Rm. 206
Washington DC 20235

Naval Air Development Center
Warminster PA 18974-5000
Attn: Commander

Naval Air Systems Command HQ
Washington DC 20361-0001
Attn: Commander

Naval Civil Engineering Laboratory
Port Hueneme CA 93043
Attn: Commanding Officer

Naval Coastal Systems Center
Panama City FL 32407-5000
Attn: Commanding Officer

Naval Facilities Engineering
Command HQ
200 Stovall St.
Alexandria VA 22332-2300
Attn: Commander

Naval Oceanographic Office
Stennis Space Center MS 39522-5001
Attn: Commanding Officer

Naval Oceanography Command
Stennis Space Center MS 39529-5000
Attn: Commander
G. Dupont
J. Boatman

Naval Oceanographic & Atmospheric
Research Laboratory
Atmospheric Directorate
Monterey CA 93943-5006
Attn: Code 400

Naval Oceanographic & Atmospheric
Research Laboratory
Stennis Space Center MS 39529-5004
Attn: Code 100
Code 104
Code 105
Code 115
Code 125L (10)
Code 125P
Code 125EX
Code 200
Code 300

Naval Oceanographic & Atmospheric
Research Laboratory
Liaison Office
Crystal Plaza #5, Rm. 802
2211 Jefferson Davis Hwy.
Arlington VA 22202-5000
Attn: B. Farquhar

Naval Ocean Systems Center
San Diego CA 92152-5000
Attn: Commander

Naval Postgraduate School
Monterey CA 93943
Attn: Superintendent

Naval Research Laboratory
Washington DC 20375
Attn: Commanding Officer

Naval Sea Systems Command HQ
Washington DC 20362-5101
Attn: Commander

Naval Surface Weapons Center Det
Silver Spring
White Oak Laboratory
10901 New Hampshire Ave.
Silver Spring MD 20903-5000
Attn: Officer in Charge
Library

Naval Surface Weapons Center
Dahlgren VA 22448-5000
Attn: Commander

Naval Underwater Systems Center
Newport RI 02841-5047
Attn: Commander

Naval Underwater Systems Center Det
New London Laboratory
New London CT 06320
Attn: Officer in Charge

Office of Naval Research
800 N. Quincy St.
Arlington VA 22217-5000
Attn: Code 10D/10P, Dr. E. Silva
Code 112, Dr. E. Hartwig
Code 12
Code 10

Office of Naval Research
ONR European Office
Box 39
FPO New York 09510-0700
Attn: Commanding Officer

Office of Naval Technology
800 N. Quincy St.
Arlington VA 22217-5000
Attn: Code 20, Dr. P. Selwyn
Code 228, Dr. M. Briscoe
Code 234, Dr. C. Votaw

Scripps Institution of Oceanography
University of California
P.O. Box 6049
San Diego CA 92106

Space & Naval Warfare Sys Com
Director of Navy Laboratories
SPAWAR 005
Washington DC 20363-5100

Space and Naval Warfare Sys Com
4455 Overlook Ave., SW
Washington DC 20375
Attn: Commander

Woods Hole Oceanographic Institution
P.O. Box 32
Woods Hole MA 02543
Attn: Director

REPORT DOCUMENTATION PAGE

Form Approved
OMB No. 0704-0188

1. Agency Use Only *(Leave blank).*	2. Report Date.	3. Report Type and Dates Covered.
	May 1991	Final

4. Title and Subtitle.

Multispectral Software Development for the Airborne Bathymetric Survey System

5. Funding Numbers.

Program Element No.	63701B
Project No.	00101
Task No.	401
Accession No.	DN794437

6. Author(s).

Maria T. Kalcic and Steve C. Lingsch

7. Performing Organization Name(s) and Address(es).

Naval Oceanographic and Atmospheric Research Laboratory
Ocean Science Directorate
Stennis Space Center, Mississippi 39529-5004

8. Performing Organization Report Number.

NOARL Report 17

9. Sponsoring/Monitoring Agency Name(s) and Address(es).

10. Sponsoring/Monitoring Agency Report Number.

11. Supplementary Notes.

12a. Distribution/Availability Statement.

Approved for public release; distribution is unlimited. Naval Oceanographic and Atmospheric Research Laboratory, Stennis Space Center, Mississippi 39529-5004.

12b. Distribution Code.

13. Abstract *(Maximum 200 words).*

The Mapping, Charting, and Geodesy (MC&G) Division of the Naval Oceanographic and Atmospheric Research Laboratory's Ocean Science Directorate is the primary activity within the U.S. Navy for conducting research and development in direct support of naval MC&G requirements. The Mapping Sciences Branch of the MC&G Division was tasked to develop the algorithms and software necessary to process data and to produce bathymetry from the multispectral scanner of the Airborne Bathymetric Survey system when it becomes fully functional. The software developed for this system is called the Multispectral Image Depth Analysis System, or MIDAS. The software processes multispectral data in conjunction with laser- or boat-derived soundings to produce high-resolution bathymetric grids. The system is designed to estimate depths in clear, shallow coastal waters down to 20 m. The depth accuracies, derived from the system using boat soundings for control, ranged from 0.3 m to 1.4 m in waters extending to 3 m and 10 m, respectively. The horizontal positioning accuracy of the system was in the 25-m range, as determined from a ground survey.

14. Subject Terms.

hydrographic surveying, airborne sounding, lasers

15. Number of Pages.

49

16. Price Code.

17. Security Classification of Report.	18. Security Classification of This Page.	19. Security Classification of Abstract.	20. Limitation of Abstract.
Unclassified	Unclassified	Unclassified	None